Distributed Acoustic Sensing for Imaging Near-Surface Geology and Monitoring Traffic at Garner Valley, California

By

Chelsea Lancelle

A dissertation submitted in partial fulfillment of

the requirements for the degree of

Doctor of Philosophy

(Geoscience)

at the

UNIVERSITY OF WISCONSIN – MADISON

2016

Date of final oral examination: 08/15/2016

The dissertation is approved by the following members of the Final Oral Committee:

Herbert F. Wang, Professor, Geoscience
Dante Fratta, Associate Professor, Geological Engineering
Kurt Feigl, Professor, Geoscience
Clifford Thurber, Professor, Geoscience
Michael Cardiff, Assistant Professor, Geoscience
Jean Bahr, Professor, Geoscience

Abstract

Distributed Acoustic Sensing (DAS) is a relatively new technology that uses a fiber-optic cable as a sensor. DAS got its start in the energy industry for borehole monitoring and more recently has started being used in horizontal arrays. The DAS technique senses strain rates every 1 m over distances of up to 100 km of cable length with sampling rates as fast as 100 kHz. This dissertation uses a horizontal DAS array in Southern California to evaluate the use of DAS for imaging near-surface geology and monitoring traffic.

The first chapter uses Multichannel Analysis of Surface Waves to evaluate the response of DAS to surface waves. Dispersion curves from the DAS array match well with results from 1) other instruments at the site, 2) ambient noise correlation functions using the same DAS array, and 3) previous studies at the site. The second chapter uses the DAS array to create 2D tomographic images of the site for a number of nodal separations and the directional sensitivity of DAS is discussed. The third chapter explores the possibility of using DAS for traffic monitoring. Vehicle counts, relative amplitudes, and velocities are identified and prove DAS could be used for traffic monitoring.

Acknowledgements

First and foremost, I want to thank my advisor Herb Wang, without whom this document would never have been written. Your guidance and advice though out both my Master's and my Ph.D. has brought me to this point, and I could not have asked for a better advisor. Next, I want to thank Dante Fratta, who has acted as an unofficial second advisor to me over the last five years. Without all of your input this project would not have turned out the way it did, and I would not have laughed nearly as hard along the way. To the rest of my committee members: Kurt Feigl, Jean Bahr, Cliff Thurber, and Mike Cardiff, thank you for your invaluable input on this document.

There were a number of people outside of my committee that helped create this dissertation in one way or another. Neal Lord, thank you for both your expertise in the field and in data analysis. This research would not have been possible without you. Peter Sobol, thank you for recreating Neal's filtering technique in a program I understand. Our associates at Silixa, and especially Athena Chalari and Rumen Karaulanov, provided expertise both in the field and in data analysis. I appreciate both Robert Nigbor and James Steidl for their help in the field. To my previous office mates Ethan Castongia, Alex Baldwin, and Ashley Meulemans, thank you for always being there when I needed input/advice/a sounding board. Thanks also for your help in the field. To the rest of my fellow graduate students in the department, thank you for keeping me sane.

Without financial support this research would have been impossible. The field work was funded by the National Science Foundation grant number CMMI-0900663 (Program Director: R. Fragaszy) and the data analysis was supported by the U.S. Department of Energy (DOE) Geothermal Technologies Office (GTO) grant number DE-EE0006760 (Program Managers: E.

Metcalfe and L. Boyd). I also want to thank ConocoPhillips and Mr. and Mrs. John Morgridge for the fellowships I received.

Lastly, I want to thank my family and friends. To my parents, Joe and Cindy, thank you for letting your little girl bring all kinds of rocks into the house and for encouraging me to follow my dreams. I promise I'll get the rocks out of your house soon! To my brother, Sam, thank you for being the best little brother I could ask for. And finally to my husband Billy, your understanding and support over the last five years has been amazing. Thank you for always listening to every practice talk (even when you have no idea what I'm talking about) and for being there when I was a stressed-out graduate student. I could not have done this without you.

Contents

List of Figures

List of Tables

Chapter 1

Introduction

Distributed Acoustic Sensing (DAS) is a relatively new, emerging technology used to measure ground motion. DAS systems need only two components: an interrogator box and fiber-optic cable. DAS can use a standard fiber-optic cable, though different buffering and sheathing options are available for different studies.

The first study to use DAS was publicly introduced in 2011 at the 81st Annual Society for Exploration Geophysicists meeting (Mestayer et al. 2011). Since then it has been published mostly in conference proceedings, though more recently journal articles are being published, including Daley et al. (2013, 2015) and half of a special section of *The Leading Edge* focused on DAS (Mateeva et al. 2016). Most of the early studies using DAS were focused on DAS arrays in boreholes for borehole monitoring (e.g. Miller et al. 2012) and DAS data was often used for Vertical Seismic Profiling.

Understanding what DAS technology measures is important to understanding the results. Daley et al. (2015) used a Vertical Seismic Profiling experiment to show that DAS effectively measures strain rate

$$\frac{\partial}{\partial t}\left(\frac{\partial u}{\partial z}\right) \tag{1.1}$$

and that the ratio of fiber particle velocity

$$v = \frac{\partial u}{\partial t} = \frac{\partial u}{\partial \varphi} \tag{1.2}$$

and fiber strain

$$\varepsilon = \frac{\partial u}{\partial z} = \pm \frac{1}{c}\frac{\partial u}{\partial \varphi} \tag{1.3}$$

is given by the propagation speed along the fiber cable, *c*, with a sign used to determine the direction of propagation. For comparison with traditional seismic instruments, Bakku (2015) shows that the response of DAS measuring strain rate at a channel located at *z* is comparable to the difference in velocities measured by two vertical geophones separated by the gauge length, *L*:

$$\dot{e}_{zz}^{DAS} = \frac{v_z\left(z+\frac{L}{2}\right) - v_z\left(z-\frac{L}{2}\right)}{L} \tag{1.4}$$

While the early studies used DAS in a vertical borehole setting, later studies have started incorporating horizontal DAS arrays (e.g. Daley et al. 2013). Daley et al. labeled DAS "a seismometer per meter" and showed good correlation between DAS in a horizontal trench and co-located geophones. The first study using DAS at UW-Madison was conducted by Castongia et al. (2016) and used DAS cable on lake ice in a horizontal array. The lessons learned from the Castongia DAS array fed into planning the horizontal DAS array used in this study.

Further applications of DAS systems could include seismic "networks of opportunity." Each time a road, borehole, pipeline, or rail track is constructed or resurfaced, fiber optic cable could be laid out. When monitoring of a specific area within the "network of opportunity" is desired, the cable is already laid out and the interrogator box simply needs to be connected to the end of the fiber and data collection can begin. Some possible examples of the use of these networks of opportunity include earthquake aftershock recording and landslide monitoring as well as more engineering-focused examples such as monitoring the freeze-thaw effect on roads in the north.

The research goal of this study is to further the understanding of DAS technology and its uses for near surface imaging and traffic monitoring. Characteristics such as the sensitivity to different types of waves and the influence of array geometry are explored. First, surface wave analysis is completed for both a DAS array and traditional seismic instruments. A large, shear-

shaking source is used to generate surface waves in a desired frequency range. Then dispersion curves are created from the data for both DAS and traditional seismic instruments. Ultimately the DAS dispersion curve is inverted for a shear wave velocity profile. The profile is compared to previously published results from the same field site.

Second, tomographic analysis is completed using the DAS data using refracted body waves to determine a resolution for the array. A Vibroseis truck and hammer blows are used to excite a DAS array. Traveltime picks are made and an inverted velocity field image of the saturated refractor is determined. The impacts of the directional sensitivity and the possible combination of tomographic images and surface wave analysis is discussed.

Third, data recorded overnight is used to investigate the use of DAS for traffic monitoring. Counts of traffic during windows of time are generated and estimates of the relative size of vehicles are determined. Velocities of the vehicles are also determined. A comparison of the signature of a passing vehicle recorded on DAS and geophones is shown. Understanding a DAS array's response to passing vehicles is not only important to removing vehicle noise from a study, but it is also beneficial to understanding studies that use traffic as a seismic source as well as studies whose purpose is to monitor traffic. The "networks of opportunity" would be helpful to those who wished to monitor traffic.

The purpose of this study is to gain improved insight into DAS characteristics to better inform future studies using DAS as well as the possibility of the seismic "networks of opportunity." This knowledge is relevant to understanding future DAS results.

References

Bakku, S. K. 2015. Fracture Characterization from Seismic Measurements in a Borehole. PhD Thesis. Massachusetts Institute of Technology.

Castongia E., Wang H. F., Lord N., Fratta D., Mondanos M., and Chalari A. 2016. An Experimental Investigation of Distributed Acoustic Sensing (DAS) on Lake Ice, *Journal of Environmental and Engineering Geophysics* (under review).

Daley T. M., Freifeld B. M., Ajo-Franklin J., Dou S., Pevzner R., Shulakova V., Kashikar S., Miller D. E., Goetz J., Henninges J., and Lueth S. 2013. Field testing of fiber-optic Distributed Acoustic Sensing (DAS) for subsurface seismic monitoring, *The Leading Edge*, June 2013, 699-706.

Daley T. M., Miller D. E., Dodds K., Cook P., and Freifeld B. M. 2015. Field testing of modular borehole monitoring with simultaneous distributed acoustic sensing and geophone vertical seismic profiles at Citronelle, Alabama, *Geophysical Prospecting*, Article first published online: 2 Nov. 2015, doi: 10.1111/1365-2478.12324.

Mateeva A., Eick P., and Hollis D. 2016. Introduction to this special section: Advances in seismic sensors, *The Leading Edge*, July 2016.

Mestayer J., Cox B., Wills P., Kiyashchenko D., Lopez J., Costello M., Bourne S., Ugueto G., Lupton R., Solano G., Hill D., and Lewis A. 2011. Field trials of distributed acoustic sensing for geophysical monitoring: 81st Annual International Meeting, SEG, Expanded Abstracts, 4253-4257.

Miller D., Parker T., Kashikar S., Todorov M., and Bostick T. 2012. Vertical Seismic Profiling using a fibre-optic cable as a Distributed Acoustic Sensor, 74th EAGE Conference &

Exhibition incorporating SPE EUROPEC 2012, Copenhagen, Denmark, 4-7 June 2012, 5 pp.

Chapter 2

Using Distributed Acoustic Sensing (DAS) for Multichannel Analysis of Surface Waves (MASW) to Evaluate Ground Stiffness[1]

Introduction

Distributed Acoustic Sensing (DAS) is a recent fiber-optic sensing technology being used primarily for Vertical Seismic Profiling (VSP) in oil-and-gas reservoirs (Mateeva et al. 2014; Johannessen, Drakeley, and Farhadiroushan 2012; Madsen et al. 2013). A limited number of DAS surface deployments have been reported. These include a small, 90-meter triangular array on lake ice (Castongia et al. 2016) and a 150-meter receiver line at a carbon sequestration site (Daley et al. 2013). Larger sized arrays of several kilometers have been planned for carbon sequestration monitoring at the Archer Daniels Midland site (http://energy.gov/fe/archer-daniels-midland-company) and for geothermal reservoir characterization (PoroTomo) at Brady Hot Springs site (http://geoscience.wisc.edu/geoscience/people/ faculty/feigl/porotomo/). This paper reports results of an intermediate-sized 762-meter array with approximate dimensions of 160-by-80 meters, which served as a prototype for the PoroTomo project, by testing the application of DAS for near-surface geologic characterization using (1) active-source Multiple Channel Analysis of Surface Waves (this manuscript), (2) P-wave tomography (Lancelle et al. 2016, in preparation), and (3) Ambient Noise Tomography (ANT) (Zeng et al. 2016).

[1] Lancelle C., Baldwin J., Lord N., Fratta D., Chalari A., Wang H. F. 2016. Using Distributed Acoustic Sensing (DAS) for Multichannel Analysis of Surface Waves (MASW) to Evaluate Ground Stiffness, *Near Surface Geophysics* (under review).

Previous DAS Studies

DAS is a measurement methodology for ground motion that is similar to Distributed Temperature Sensing (DTS) (e.g., Tyler et al. 2009) or Distributed Strain Sensing (DSS) (e.g., Froggatt and Moore 1998) in that the fiber-optic cable itself is the sensor. However, rather than temperature or static strain, DAS senses vibrations along the fiber-optic length. This sensing is done by sending a short pulse of laser into the cable and monitoring returning signals from Rayleigh backscattering that occurs along the fiber (Johannessen et al. 2012). Phase changes of consecutive pulses from the same region of fiber are caused by changes in the length of a segment of fiber. The length of fiber over which the changes are measured is called the gauge length. The change in the response between two pulses is approximately linearly proportional to a change in the average fiber elongation over the gauge length. Because the DAS system compares the strain between consecutive laser pulses, the effective output of the DAS system is strain rate (Parker, Shatalin, and Farhadiroushan 2014; Daley et al. 2015). The center of the gauge length is called a channel, and for each channel a strain rate is calculated. When the fiber is coupled with a medium, the movement caused by passing waves creates a small displacement in the fiber, allowing the strain rate in the medium to be monitored (Parker et al. 2014). The DAS technique senses strain rates every 1 m over distances of up to 100 km of cable length with sampling rates as fast as 100 kHz (Johannessen et al. 2012; Madsen et al. 2013; Miller et al. 2012; Parker et al. 2014). A standard, single-mode fiber-optic cable can be used, although cables specifically made to work with DAS may improve performance (Madsen et al. 2013; Parker et al. 2014).

Several studies have utilized DAS in borehole and near-surface horizontal arrays. Daley et al. (2013) deployed fiber-optic cables in boreholes and surface trenches to monitor seismic

waves created by a drop-weight source. The cable was placed in the surface trench in order to compare the DAS data to co-located geophone responses along the fiber-optic cable. The captured data showed high-quality surface waves and they found that the cable deployed in the trench had a similar signal-to-noise ratio between co-located points on the fiber-optic cable and geophones. Hornman (2016) used a helically wound cable to test the validity of using DAS for seismic recording on land. The helically wound cable was designed to have broadside sensitivity, something a horizontal fiber lacks. The helically wound cable was placed in a shallow borehole and compared with a co-located streamer. The data from the cable showed that helically wound cable could successfully be used for seismic monitoring on land. Castongia et al. (2016) utilized a fiber-optic cable laid out in a triangular array and frozen into the ice of Lake Mendota (Madison, WI). Two types of fiber cables (i.e., tight buffered and loose-tube cables) were used and the fiber-optic cable was looped multiple times around the array to compare fiber types and the effect of signal attenuation along co-located points in the fiber. The study also assessed the directional sensitivity of the cable. Finally, collected data were used in the inversion of travel time to image the stiffness of the ice layer. Two-dimensional wave velocity tomography results for the DAS system were more robust than results from seismometers that were also deployed at the site. The improved tomographic images were simply due to higher station density allowed by close separation of channels in the DAS array.

Other researchers have also used DAS in energy exploration applications. These studies involved the deployment of fiber-optic cables in boreholes along with geophones (Johannessen et al. 2012; Madsen et al. 2013; Daley et al. 2013; 2015; Bakku 2015). In these studies, fiber-optic cables were coupled to the borehole by grout or clamped to tubing while the vibrational response was also assessed with geophones. All these studies document that quality of the signal and the

noise level are comparable to those of geophones with the advantage of a much large sensor array.

In summary, two advantages of DAS are that (1) fiber-optic cable is installed once for use in repeat surveys and (2) a single interrogator can sense hundreds or thousands of meters with spatial resolution finer than 10 meters. Limitations of DAS include that it is sensitive only to axial strain and the measurement technique limits the bandwidth to wavelengths larger than the DAS gauge length.

Multiple Channel Analysis of Surface Waves

Dispersion of surface waves occurs when they propagate in a medium with vertical stiffness distribution (Park, Miller, and Xia 1999). Waves propagate at different velocities as increasing wavelengths sense greater depths with different stiffness. If the wave velocity increases with depth, this phenomenon means that lower-frequency phases propagate at higher phase velocities. On the other hand, shorter wavelength phases tend to travel more slowly, because they are only passing through the near-surface material that has lower wave velocity. Surface-wave techniques use the dispersive response of Rayleigh and Love waves in vertically heterogeneous media to invert for the S-wave velocity distribution versus depth. The results of the dispersion analyses are then used to determine the stiffness and dynamic behavior of near-surface formations and to study geological structures.

Active and passive sources of surface waves are used in geological and geotechnical engineering applications to assess the dynamic properties of the near surface (Picozzi et al. 2009; Foti et al. 2015). The active techniques, which use seismic sources such as a hammer impact or Vibroseis, are Spectral Analysis of Surface Waves (SASW) (Rix, Stokoe, and Roesset 1991) and

Multiple Channel Analysis of Surface Waves (MASW) (Park et al. 1999; Miller et al. 1999). Passive techniques are Refraction Microtremors (ReMi) (Louie 2001) and Ambient Noise Tomography (ANT) (Lin et al. 2007). In the case of SASW, two sensors capture the phase velocity as a function of frequency of a propagating surface wave by performing a spectral analysis of the captured signals (Rix et al. 1991). In the case of MASW, multiple channels capture the arrival of surface waves. By applying narrow-band filters and following the moveout of a particular phase between different sensors, the phase velocity is obtained at different frequencies from which a high-quality surface-wave dispersion curve can be determined (Park et al. 1999).

The two active-source techniques have advantages and disadvantages. The main advantage of SASW is that only two sensors are needed. However, in order to create a dispersion curve, many frequencies need to be sampled, and that may require reconfiguring of the sensors in the field by changing the separations of both sensors and seismic sources, which can make the process time and labor-intensive. Moreover, the SASW method assumes that only fundamental mode surface waves exist in the field (Rix et al. 1991) and therefore other propagation modes may be missed with the use of only two sensors. The MASW technique was first described by Park et al. (1999). MASW overcomes some of the disadvantages in SASW. The use of multiple sensors allows for multiple propagation modes to be identified. It also allows for less time in the field between source locations because reconfiguring the sensors is not required (Park et al. 1999). Increasing the number of sensors used in MASW allows for more straightforward identification of propagation modes.

Study Area

In September 2013 the DAS trial was conducted at the George E. Brown Jr. Network for Earthquake Engineering Simulation (http://nees.ucsb.edu/facilities/GVDA) Garner Valley Downhole Array (GVDA) field site in Southern California. The GVDA is 20 km southwest of Palm Springs, California, USA. It is located in a seismically active region 7-km east of the San Jacinto fault and 35-km west of the San Andreas Fault (Fig. 2.1 inset). The geology of the site is well known and the local sediments have been fully characterized with geotechnical engineering logs (Youd, Bartholomew, and Proctor 2004) and with surface-wave analysis (Stokoe, Kurtulus, and Menq 2004). From a fairly flat surface to about 16-m depth, the subsurface is composed mostly of silty and sandy soils. Below that is weathered granite to a depth of about 90 meters, and that is underlain by granite bedrock (Fig. 2.2). The water table is located at about 5-m depth but it changes seasonally by a few meters.

At the site 762-meter-long fiber-optic cable was laid in a trench at a depth of about 0.3 m in a rectangular design with two interior diagonal segments (Fig. 2.1). The approximately rectangular perimeter measures about 160 m by 80 m. The trench was backfilled and left for three months during which sandy soil settled back into the trench, effectively coupling the cable with the ground. An Optical Cable Corporation fiber-optic cable with two single-mode and two multi-mode tightly-buffered fibers in the same jacket was used in the study. The two single-mode fibers were spliced together at the end of the line to allow for two co-located measurements at each meter of fiber.

Existing sensors at the field site include two GVDA surface accelerometers that were used in this study (details at http://nees.ucsb.edu/facilities/GVDA). A 48-channel seismometer array was deployed. It consisted of two Geometrics GEODE 24-channel seismographs provided

by the IRIS Program for Array Seismic Studies of the Continental Lithosphere (PASSCAL) together with 18 tri-axial 4.5 Hz L-28-3D geophones (details at https://www.passcal.nmt.edu/content/instrumentation/sensors). Eight of the geophones were positioned five-meters apart on the first diagonal segment and the other ten geophones were placed along the second diagonal segment. Of those ten geophones, six of them were monitoring only the vertical component of ground motion. Seven UCLA (http://nees.ucla.edu/sensors.html) tri-axial accelerometers were used to monitor the source on the Mini-Me structure, a one-story tall structure, which was built to assess the response of simple structures to local seismic excitation (http://nees.ucsb.edu/facilities/GVDA).

Seismic Sources

Active Source: The active source used in this field test was a stationary 45-kN eccentric mass shaker located exterior to the DAS array on top of the Mini-Me structure (Fig. 2.1). The shaker was swept from DC to 10 Hz and back to DC over a 60-second excitation period. This sweep was followed by a 3-second listening time, making the length of each file 63 seconds long. Resonance of the Mini-Me structure was reached at around 5 Hz, creating a small deviation from the otherwise linear excitation sweep. External triggering was used to synchronize the source and the PASSCAL and DAS systems. Ten repetitions of the source at 100 percent power were run to vibrate the structure and excite the field. The shaker sweep generated vertically-polarized shear waves. The shear waves radiated energy mainly in the west-to-east direction. MASW has been used previously with a mass shaker similar to UCLA's for monitoring carbon sequestration (Ikeda et al. 2015).

Passive Source: California Highway 74 runs parallel to the main axis of the DAS array at the Garner Valley test site (Fig. 2.1). Highway traffic creates vibrations that were sensed throughout the deployed sensor array. The number of passing vehicles was recorded for each test because traffic has the potential to add noise to the recorded data. On the other hand, traffic noise could be used as a seismic source using Noise Correlation (NCF) analysis (Nakata et al. 2011, Zeng et al. 2016).

Surface-Wave Dispersion Analysis

The main objective in the surface-wave analysis is the creation of the dispersion curve; that is, obtaining phase velocities for multiple frequencies in the surface wave. Thus, MASW requires that the traces received from a swept-frequency source are filtered for specific frequencies over a range of frequencies (Park et al. 1999). Generally, this can be done by using a sequence of band-pass filters to determine the propagating velocity for specific frequencies. In this study, the phase velocity of individual frequencies was obtained using a modified version of MASW incorporating Moving Window Cross Correlation (MWCC) (Sun, Milkereit, and Schmitt 2009).

Two processing steps were performed on the receiver traces. First, a Source Synchronous Filter (SSF) (Lord, Wang, and Fratta 2016) was applied to all the receiver traces. The SSF was developed for a swept-frequency source to remove out-of-band noise and unwanted source harmonics. The SSF is a narrow-band filter synchronized with the source frequency, which for the Mini-Me shaker was taken to be an idealized sweep from DC to 10 Hz and back to DC linearly over 60 seconds. The narrow-band filter had a bandwidth of 2 Hz to account for the time-varying source function and the maximum travel-time delay (less than one second) for

surface waves propagating across the array. The largest sources of noise removed by the SSF are the source harmonic and passing vehicles. The SSF was applied to all receiver signals before further analysis. For the PASSCAL geophones, a pole-zero compensation was applied to remove the 4.5 Hz geophone response and Automatic Gain Control (AGC) was applied to reduce amplitude variations in all data.

Following the SSF processing, MWCC was applied to the processed time-domain traces. For MWCC a small, tapered time window of the source waveform (with its restricted range of frequency) is cross-correlated with a set of receiver signals over a range of distances. The source waveform used in the MWCC technique is the north-south component of one of the UCLA accelerometers on top of the Mini-Me structure. The source window is filtered to remove high-frequency noise and harmonics using SSF prior to the cross correlation. A particular peak of the cross-correlation function was tracked for a range of receiver distances. The slope of the line is the phase velocity for the frequency of the source within the small time window.

The final step in MASW analysis is to invert the dispersion curve for a shear-wave velocity profile. In this study we use the Surface Wave Modal Inversion (SWAMI) tool (Lai and Rix 1998). The required inputs to SWAMI are the number of layers and their thicknesses, densities, and Poisson's Ratios, as well as the frequencies and corresponding velocities from the dispersion curves.

Results

The analysis was completed for two different sections of cable shown in Fig. 2.1. One of the sections of cable is aligned with the PASSCAL sensors on one of the diagonals, referred to as the "cross hatch." Results from this section of cable are plotted with results determined from the

PASSCAL geophones on the same diagonal section. Fig. 2.3 shows normalized data from one 45-kN shaker test for both one DAS channel and a co-located PASSCAL geophone. An accelerometer on the source structure is also plotted. Passing vehicles can be seen in the data both at the beginning and the end of the sweep. The other section of cable is on the long, radial line from the large shear shaker, referred to as the "long line." Results from this line are compared to results calculated from GVDA accelerometers along the same line. Fig. 2.4 shows a plot over 30 meters of raw DAS data as well as filtered data that was processed using SSF. Almost all noise from the passing vehicle is removed.

Of all the different excitations, the shake with the fewest number of passing vehicles was chosen for the analysis presented herein to help reduce the effect traffic noise on the signal. Only the upsweep of the source from 2 to 10 Hz was used to create the dispersion curves, as this allowed the different phases to spread out rather than overtake each other as lower frequencies have higher phase velocities. Below 2 Hz, the energy of the source was too low to obtain a coherent phase, so those frequencies did not contribute to the dispersion curve.

Multiple time windows were tested as the source window for the MWCC portion of the MASW analysis. The source-time windows used for cross-correlation were six seconds wide, corresponding to a frequency width of 2 Hz. The source windows were spaced every 1.5 s, meaning the frequency shifted by 0.5 Hz between each window. The source windows were tapered using a Tukey cosine window. The power spectral density of each windowed signal was taken to determine the dominant frequency. These tapered and windowed signals were then cross-correlated with the vertical component of the seismometers, accelerometers, and the DAS array responses.

Fig. 2.5 shows plots of data from 30 meters of fiber optic cable from the DAS array. Frequencies of 2, 4, 6, and 8 Hz are shown and the moveout of each phase is marked. Clear moveout is seen for all four frequencies. Fig. 2.6 shows the experimental dispersion curve for the DAS array's long line as well as the GVDA accelerometer sensors 8 and 10 along the same line. Fig. 2.7 shows dispersion curve results for the cross hatch section of the DAS cable, as well as the PASSCAL geophone results from the same line.

The dispersion curve from the DAS long line was inverted to develop a shear-wave velocity profile of the site using SWAMI. The resulting shear-wave velocity profile is shown in Fig. 2.8. All input parameters for the SWAMI model were based on the values for the SASW highway line from Stokoe et al. (2004) (Table 2.1).

Discussion

The response of a DAS channel is not a point measurement but is a spatial average over its gauge length. The gauge length used in this study was 10 meters. Each channel's strain-rate value is obtained as an average over a 10-m segment of cable whose center location is the designated channel. Then the 10-m segment shifts one meter to represent the next channel. Possible aliasing could arise if the seismic wavelengths were less than 20 meters. In our study wavelengths are generally greater than 20 meters but near 10 Hz, the upper range of our frequencies, the wavelength falls to about 18 meters. Also, the gauge length of 10 meters means that nearby channels share part of the cable segment over which the strain rate is obtained. Thus, the channels spaced 5-m apart and plotted in Fig. 2.5 are sharing 5 meters of sampling length between them. Nonetheless, clear moveout is seen for the 5-m separation and clear time

differences in the arrivals of phases are seen when every channel spaced one meter apart is plotted.

Figs. 2.5 and 2.6 compare results from lines of the DAS array with the corresponding PASSCAL geophones and GVDA accelerometers. In all cases, the general relationship between phase velocity and frequency is the same and in agreement with the general observation that velocity tends to decrease with increasing frequency. When looking at results from the long line in Fig. 2.6, the curves match within about 10 m/s but with the exception of a deviation between the two curves for frequencies between 4 and 6 Hz. This deviation may be linked to a number of factors. One possibility is an effect due to the resonance of the structure at about 5 Hz. When the structure hits resonance, it may be introducing more complex waveforms into the ground, complicating the dispersion curve as well. The larger number of DAS channels means that the signal was still clearly identifiable from the noise. Having only two accelerometers made this identification more difficult and thus the results may have been more affected by the resonance of the structure. A second possibility for the difference relates to a phase shift that is seen in the data. There appears to be interference between different propagation modes that is most prominent for frequencies between 4 and 6 Hz. When the interference occurs, only channels away from the phase shift were used to avoid apparent velocity changes due to the phase shift. However, the mode interference may still be causing a perturbation in the velocities near those frequencies. The denser spatial sampling of DAS allowed a better understanding of the different propagation modes. The interference between the modes was not seen in the accelerometer data because of the small number of stations. The interference would not have been apparent without the DAS data. Finally, a third possibility for the difference in the dispersion curves relates to differences in sensor orientation. Surface-wave analysis generally uses measurements from

vertically-oriented seismometer components, so that is what was used in this study for those sensors. However, DAS is sensitive to axial strain along the length of the fiber (Mateeva et al., 2014). The fiber-optic cable along the long line will be most sensitive to motion in the radial direction away from the Mini-Me source.

Fig. 2.7 shows results from the cross-hatch segment of cable adjacent to the PASSCAL geophones. Here the agreement between PASSCAL geophones and DAS array is not as strong and the velocities are different by up to 200 m/s for low frequencies, though the results do agree within 20 m/s or less for frequencies above 6 Hz. The cross-hatch segment of cable tends to have lower velocities at lower frequencies than the geophones. The differences at low frequencies may be due to the possibilities listed previously for the long line. The difference in agreement between DAS and conventional sensors lines for the two line segments is likely because the long line is oriented radially away from the source, whereas the other line adjacent to the PASSCAL sensors is at an angle with respect to the propagation direction. Issues for all of these dispersion curves could arise from misidentification of the arrival time due to interference between waves along the cable.

DAS dispersion curve results are compared in Fig. 2.8 with those from a previous study at the site by Stokoe et al. (2004) for which a large Vibroseis truck was used as the source. Results were obtained using the SASW method for two lines - one by the parking lot and one by the highway (Fig. 2.1). The dispersion curves from both lines are plotted along with the dispersion curves from the DAS results. Only comparisons will be made with the highway line because the parking lot line is across a poorly-graded gravel layer which is inconsistent with the rest of the site and yielded increase variability in Stokoe et al.'s results. The DAS results from the long line of cable match those of Stokoe et al.'s highway line within an average of 20 to 30

m/s. The differences between the two data sets may be due to the different techniques used, to site heterogeneity, and to different depths of the water table at the time of the tests. Other differences were that Stokoe and co-workers used SASW with a Vibroseis source, while we utilized MASW with a stationary shear-shaker source. It is also possible that the site conditions were different between the two tests. Changes in moisture in the soil and depth to water table may also account for some of the small differences between the dispersion curves. The cross-hatch line results do not match the Stokoe et al. results as well. Again, this could be due to a difference in site heterogeneity, site conditions, or technique, but it could also be due to any of the reasons listed for the differences between DAS with the PASSCAL geophone data.

The shear-wave velocity profile calculated from the DAS long-line dispersion curve is compared with that obtained from Stokoe et al.'s highway line in Fig. 2.9. Only velocities for frequencies below 10 Hz were used from the Stokoe et al. dispersion curve. At less than 5-m depth a comparison of the results is not reliable because a difference in water content in the soil is possible between this study and the one by Stokoe et al., which could affect the velocities calculated that near the surface. Both profiles show increasing velocity with depth once below 5 meters, but the velocity values do not agree in detail. These differences are associated with differences in the dispersion curves as well as the non-uniqueness inherent in surface-wave inversions (Foti et al. 2009).

Results from borehole geophysical logs at the site by Steller (1996) are plotted in Fig. 2.9 for comparison with both inversion results. Near the surface the comparison is again unreliable due to a possibility of differences in water content in the soil. For the layer approximately 6 to 17 meters depth both inversions match the measured velocity within 25 m/s. Both of the

inversions underestimate the velocity in the next layer, and in the final, deepest layer the Stokoe et al. velocity is a better match on average than that of the DAS value.

Finally, the active-source results are compared with those derived from using traffic noise as a source. Zeng et al. (2016) used 8 hours of continuous overnight recording from the same DAS array presented in this study to calculate a dispersion curve based on noise cross-correlation functions (NCFs). The prevailing source of noise during the overnight recording was traffic passing on Highway 74. The dominant frequencies from traffic were between 5 and 25 Hz. The NCFs for one-minute intervals were stacked using phase-weighted stacking to improve the signal. Then MASW was used to calculate a dispersion curve from the NCFs and the results are plotted along with results from the long line in this study in Fig. 2.10. Only the results from frequencies between 6 and 10 Hz were plotted since the frequencies used in the Zeng paper were from 5 to 25 Hz. The results from the passive overnight recording match within 10 m/s with those from the active tests used in this study; thus DAS was successfully used in both a passive and active manner to obtain the same results.

Conclusions

A field test was conducted in September 2013 in Garner Valley, California where a DAS array as well as seismometers and accelerometers were deployed. A 45-kN, swept-frequency shear shaker excited the field between 2 and 10 Hz. Multiple sensors are inherent to a DAS array making it very well suited to Multichannel Analysis of Surface Waves (MASW) analysis to obtain surface-wave dispersion curves. The results from DAS agree with those from the traditional seismic sensors as well as results from previous studies at the same site. The DAS results also match within 10 m/s with results using Noise Correlation Functions (NCF) from

traffic noise using the same array. Differences in results could be attributed to differences in the number of sensors, in the response associated with a hitch in the source output at the resonant frequency of the structure on which the source was located, in sensing orientation of the receivers, or to multimode wave interference.

References

Bakku, S. K. 2015. Fracture Characterization from Seismic Measurements in a Borehole. PhD Thesis. Massachusetts Institute of Technology.

Castongia E., Wang H. F., Lord N., Fratta D., Mondanos M., and Chalari A. 2016. An Experimental Investigation of Distributed Acoustic Sensing (DAS) on Lake Ice, *Journal of Environmental and Engineering Geophysics* (under review).

Daley T. M., Freifeld B. M., Ajo-Franklin J., Dou S., Pevzner R., Shulakova V., Kashikar S., Miller D. E., Goetz J., Henninges J., and Lueth S. 2013. Field testing of fiber-optic Distributed Acoustic Sensing (DAS) for subsurface seismic monitoring, *The Leading Edge*, June 2013, 699-706.

Daley T. M., Miller D. E., Dodds K., Cook P., and Freifeld B. M. 2015. Field testing of modular borehole monitoring with simultaneous distributed acoustic sensing and geophone vertical seismic profiles at Citronelle, Alabama, *Geophysical Prospecting*, Article first published online: 2 Nov. 2015, doi: 10.1111/1365-2478.12324.

Foti S., Comina C., Boiero D., and Socco L. V. 2009. Non-uniqueness in surface-wave inversion and consequences on seismic site response analyses, *Soil Dynamics and Earthquake Engineering*, 29(6), 982-993.

Foti S., Lai C., Rix G. L., and Strobia C. 2015. *Surface Wave Methods for Near Surface Wave Characterization*, CRC Press, Boca Raton, FL. 467 pages.

Froggatt M. and Moore J. 1998. High-spatial-resolution distributed strain measurement in optical fiber with Rayleigh scatter, *Applied Optics* 37, 1735-1740.

Hornman J.C. 2016. Field trial of seismic recording using distributed acoustic sensing with broadside sensitive fibre-optic cables, *Geophysical Prospecting*. doi: 10.1111/1365-2478.12358

Ikeda T., Tsuji T., Watanabe T., and Yamaoka K. 2015. Development of a surface-wave monitoring system for leaked CO_2 using a continuous and controlled seismic source, *International Journal of Greenhouse Gas Control*, 45(2016), 94-105.

Johannessen K., Drakeley B., and Farhadiroushan M. 2012. Distributed Acoustic Sensing - a new way of listening to your well/reservoir, *SPE Intelligent Energy International* held in Utrecht, The Netherlands, 27–29 March 2012, SPE 149602, 9 pp.

Lai C. G., and Rix G. J. 1998. Simultaneous inversions of Rayleigh phase velocity and attenuation for near-surface site characterization, Report No. GITCEE/GEO-98-2, School of Civil and Environmental Engineering, Georgia Institute of Technology, 258 pp.

Lin F. C., Ritzwoller M., Townend J., Bannister S., and Savage M. 2007. Ambient noise Rayleigh wave tomography of New Zealand, *Geophysical Journal International*, 170, 649-666.

Lord N., Wang H. F., and Fratta D. 2016. A Source-Synchronous Filter for Uncorrelated Receiver Traces from a Swept-Frequency Seismic Source, *Geophysics* (in press).

Louie J. N. 2001. Faster, Better: Shear-Wave Velocity to 100 Meters Depth from Refraction Microtremor Arrays, *Bulletin of the Seismological Society of America*, 91(2), 347–364.

Madsen K.N., Dümmong S., Kritski A., Pedersen Å.S., Finfer D., Gillies A., and Travis P. 2013. Simultaneous Multiwell VSP in the North Sea Using Distributed Acoustic Sensing, 75th EAGE Conference & Exhibition incorporating SPE EUROPEC 2013, London, UK, 10-13 June 2013, 5 pp.

Mateeva A., Lopez J., Potters H., Mestayer J., Cox B., Kiyashchenko D., Wills P., Grandi S., Hornman K., Kuvshinov B., Berlang W., Yang Z., and Detomo R. 2014. Distributed acoustic sensing for reservoir monitoring with vertical seismic profiling, *Geophysical Prospecting*, 62, 679–692, doi: 10.1111/1365-2478.12116.

Miller D., Parker T., Kashikar S., Todorov M., and Bostick T. 2012. Vertical Seismic Profiling using a fibre-optic cable as a Distributed Acoustic Sensor, 74th EAGE Conference & Exhibition incorporating SPE EUROPEC 2012, Copenhagen, Denmark, 4-7 June 2012, 5 pp.

Miller R. D., Xia J., Park C. B., and Ivanov J. M. 1999. Multichannel Analysis of Surface Waves to map bedrock, *The Leading Edge*, 18(12), 1392-1396.

Nakata N., Snieder R., Tsuji T., Larner K., and Matsuoka T. 2011. Shear wave imaging from traffic noise using seismic interferometry by cross-coherence, *Geophysics*, 76(6), SA97–SA106, doi: 10.1190/GEO2010-0188.1

Park C. B., Miller R. B., and Xia J. 1999. Multichannel analysis of surface waves, *Geophysics*, 64(3), 800–808.

Parker T., Shatalin S. V., and Farhadiroushan M. 2014. Distributed Acoustic Sensing - A new tool for seismic applications. *First Break*, February 2014, 61-69.

Picozzi M., S., Parolai, Bindi D., and Strollo A. 2009. Characterization of shallow geology by high-frequency seismic noise tomography, *Geophysical Journal International*, 176, 164–174 doi: 10.1111/j.1365-246X.2008.03966.x

Rix G, Stokoe K. H., and Roesset J. M. 1991. *Experimental Study of Factors Affecting the Spectral-Analysis-of-Surface-Waves Method*, Center for Transportation Research, The University of Texas at Austin, Research Report 1123-5. URL: http://library.ctr.utexas.edu/digitized/texasarchive/phase2/1123-5.pdf [Accessed on January 9, 2016].

Steller R. 1996. *New Borehole Geophysical Results at GVDA*, Data Report.URL: http://nees.ucsb.edu/sites/eot-dev.nees.ucsb.edu/files/facilities/docs/GVDA-Geotech-Stellar1996.pdf [Accessed on June 9, 2016].

Stokoe K. H., Kurtulus A., and Menq F.-Y. 2004. *Data Report: SASW Measurements at the NEES Garner Valley Test Site, California*, 13 January 2004, 12 pp.

Sun L. F., Milkereit B., and Schmitt D. R. 2009. Measuring velocity dispersion and attenuation in the exploration seismic frequency band, *Geophysics*, 74(2), 113-122.

Tyler S. W., Selker J. S., Hausner M. B., Hatch C. E., Torgersen T., and Schladow S. 2009. Environmental Temperature Sensing Using Raman Spectra DTS Fiber-Optic Methods, *Water Resources Res.*, 4(187), 673-679.

Youd T. L., Bartholomew H. A. J., and Proctor J. S. 2004. *Geotechnical logs and data from permanently instrumented field sites: Garner Valley Downhole Array (GVDA) and Wildlife Liquefaction Array (WLA)*, Data Report.URL: http://nees.ucsb.edu/sites/eot-dev.nees.ucsb.edu/files/facilities/docs/geotech-data-report.pdf [Accessed on January 9, 2016].

Zeng X., Lancelle C., Thurber C., Fratta D., Wang H. F., Lord N., Chalari A., and Clarke A. 2016. Properties of Noise Cross-correlation Functions Obtained from a Distributed Acoustic Sensing Array at Garner Valley, California, *Bulletin of the Seismological Society of America* (under review).

Figures

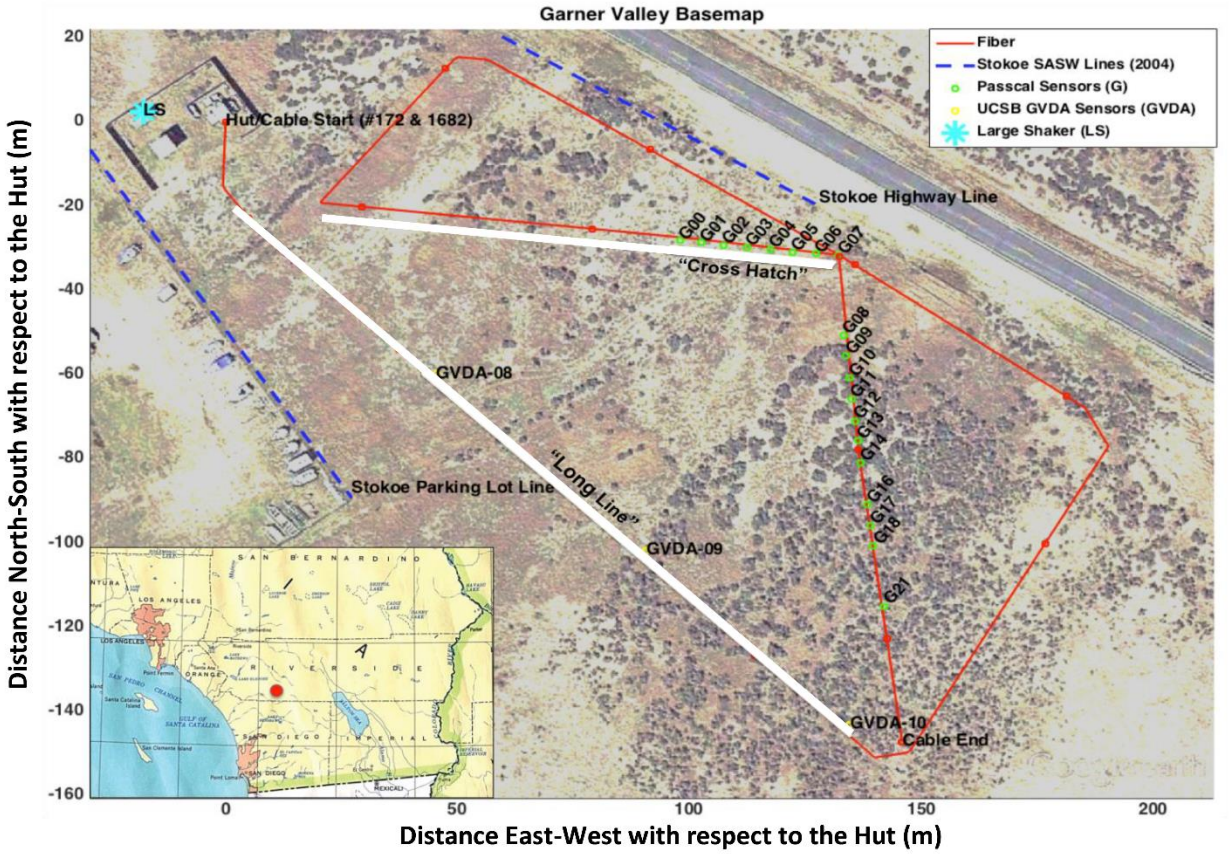

Figure 2.1: Map of the Garner Valley field site. The red line is the layout of the fiber. The two fibers in the same jacket are spliced together at the cable end to create two measurement points at each channel location. The highway runs parallel to the long axis of the array and it is the main source of noise. White lines denote the "Cross Hatch" and "Long Line" segments of fiber. Locations of Stokoe *et al*. (2004) lines as well as locations of PASSCAL geophones and GVDA accelerometers are also shown. Inset shows location of the field site in Southern California.

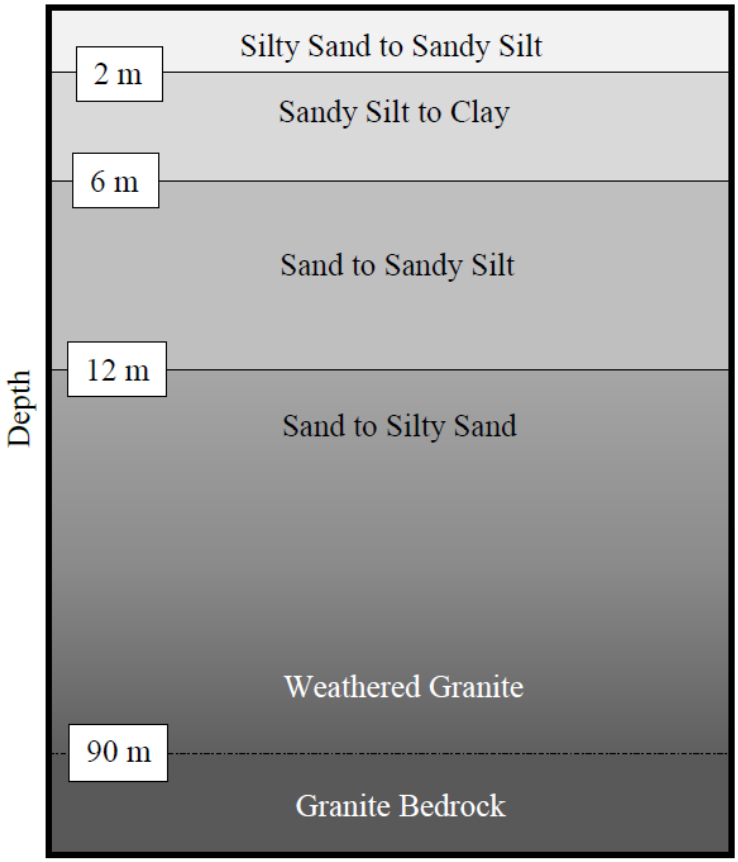

Figure 2.2: Basic cross-section of the geology of the site. Not to scale, depths are approximate.

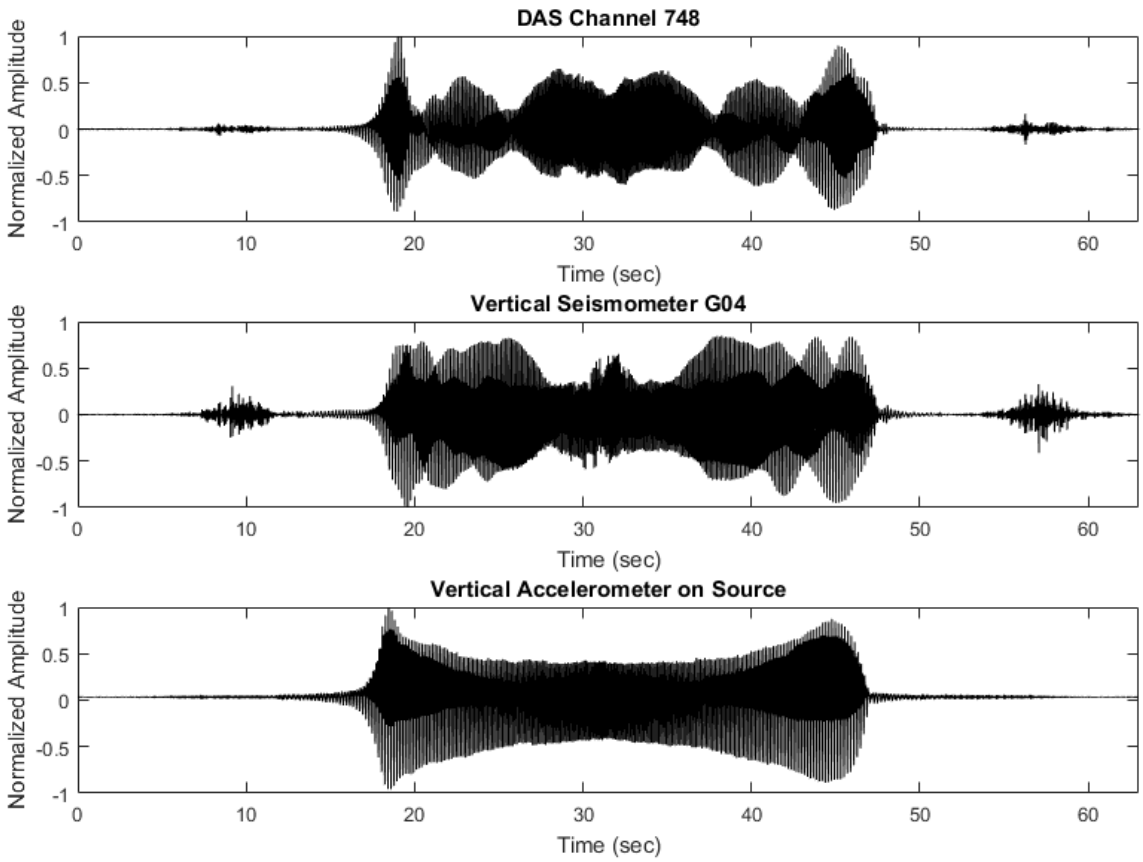

Figure 2.3: Plots of data for a co-located DAS channel (top) and vertical seismometer component (middle). The bottom plot shows a vertical component from one of the accelerometers on the Mini-Me source structure. All three amplitudes have been normalized. Noise in both the DAS and seismometer plots at around 10 and 57 seconds are from passing vehicles on Highway 74.

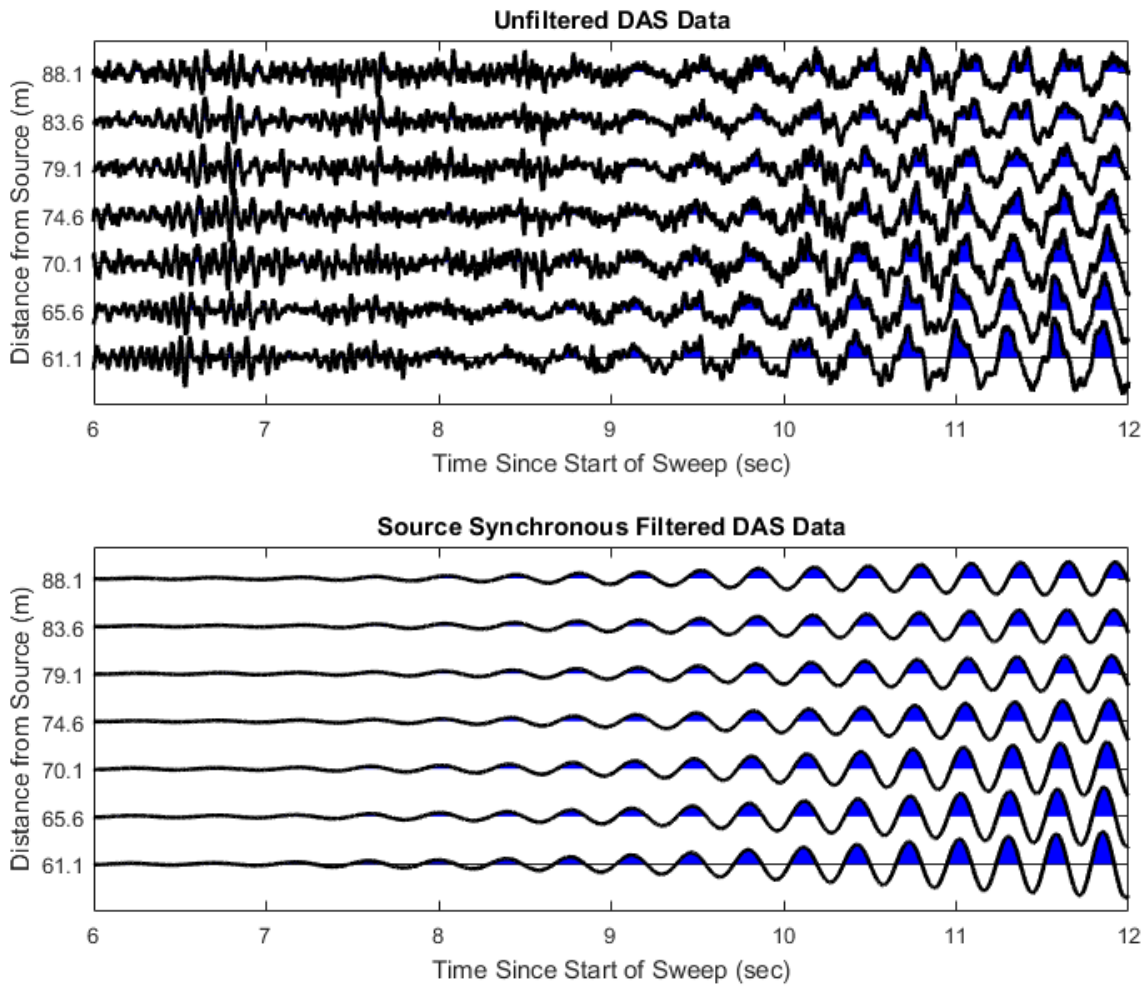

Figure 2.4: (Top) Plot of 30 m of unfiltered DAS data. Channels are spaced 5 m apart and distances to the 45-kN source are given. The source was sweeping from 2 to 4 Hz during this time window. A passing vehicle arrival can be seen around 6.5 seconds. (Bottom) Source synchronous filtered DAS data plotted over the same 30 m and the same time interval. Source harmonics and traffic noise are removed.

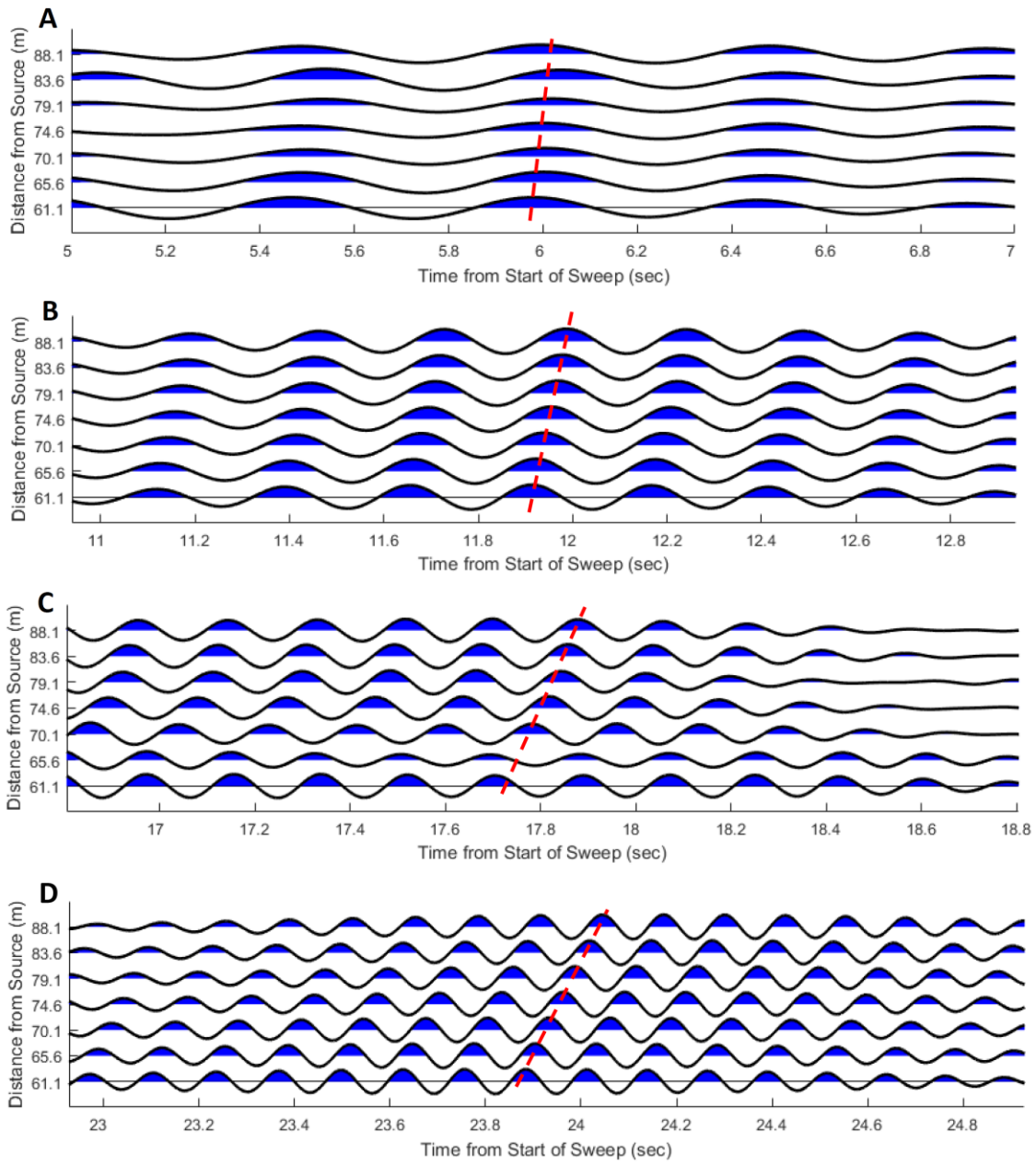

Figure 2.5: Plots A-D show source synchronous filtered MWCC DAS data at frequencies of 2, 4, 6, and 8 Hz with approximate velocities of 710, 360, 250, and 200 m/s respectively. 30 meters of cable are shown with every fifth channel plotted. Distance from the 45 kN shaker source is shown. The frequencies are based on what the source was outputting at that time assuming a

linear sweep (e.g. at 6 seconds the source was outputting 2 Hz). The dashed line follows the move-out of a phase. Notice the slope of the line gets steeper as the frequency decreases.

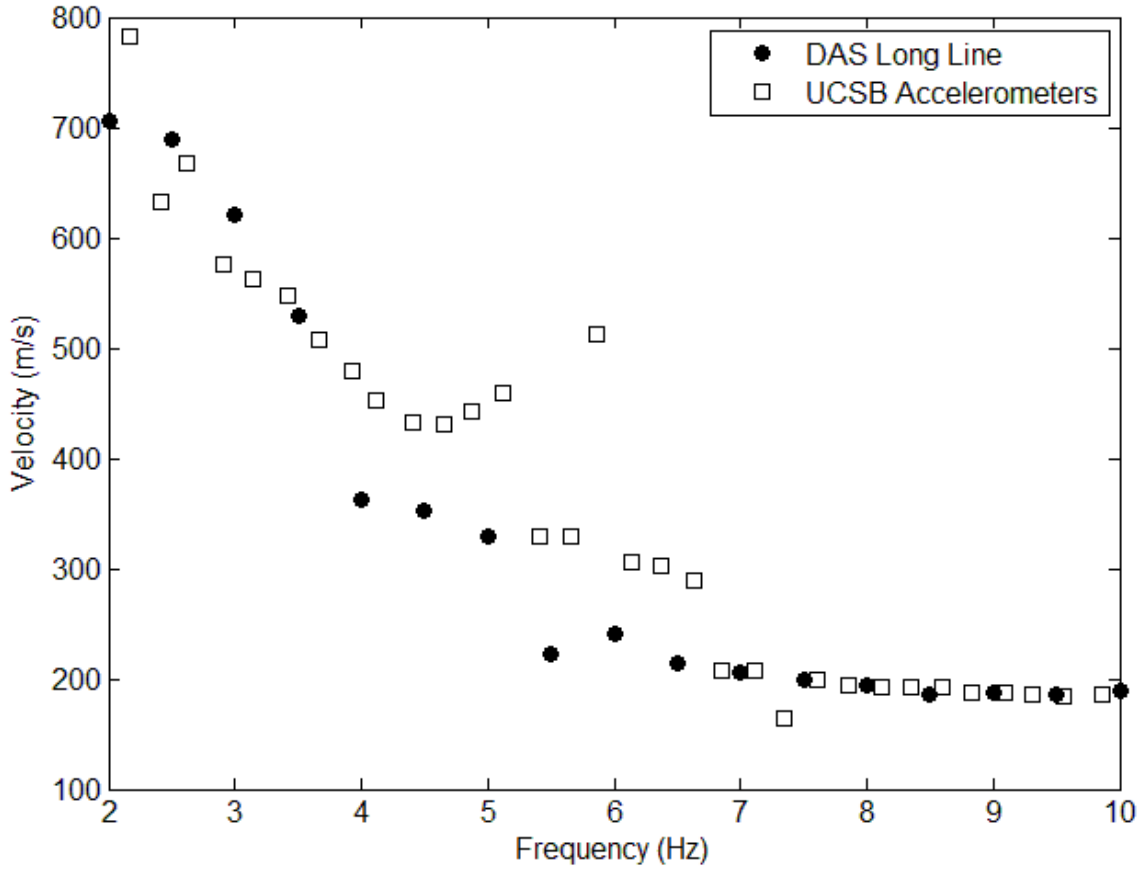

Figure 2.6: Dispersion curve results for the DAS long line and the GVDA accelerometers numbered 8 and 10.

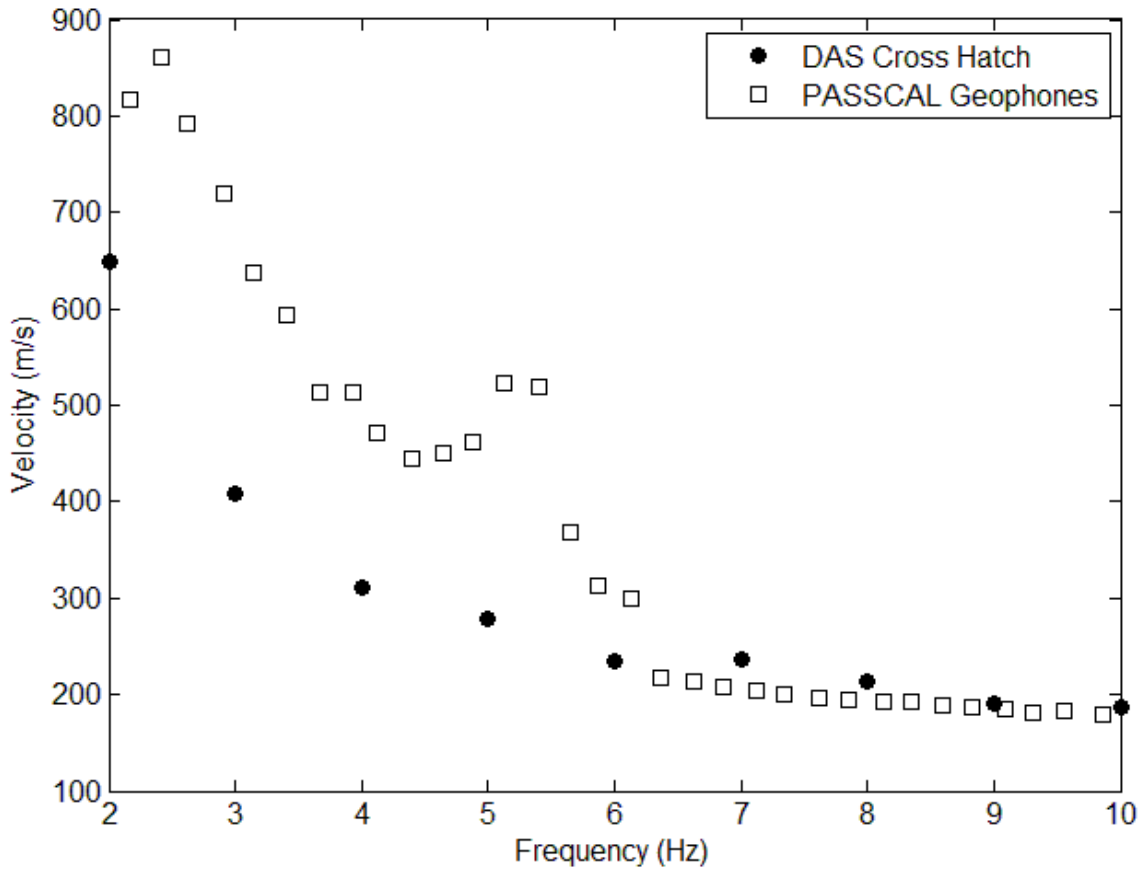

Figure 2.7: Dispersion curve results from the DAS cross hatch line as well as the PASSCAL geophones.

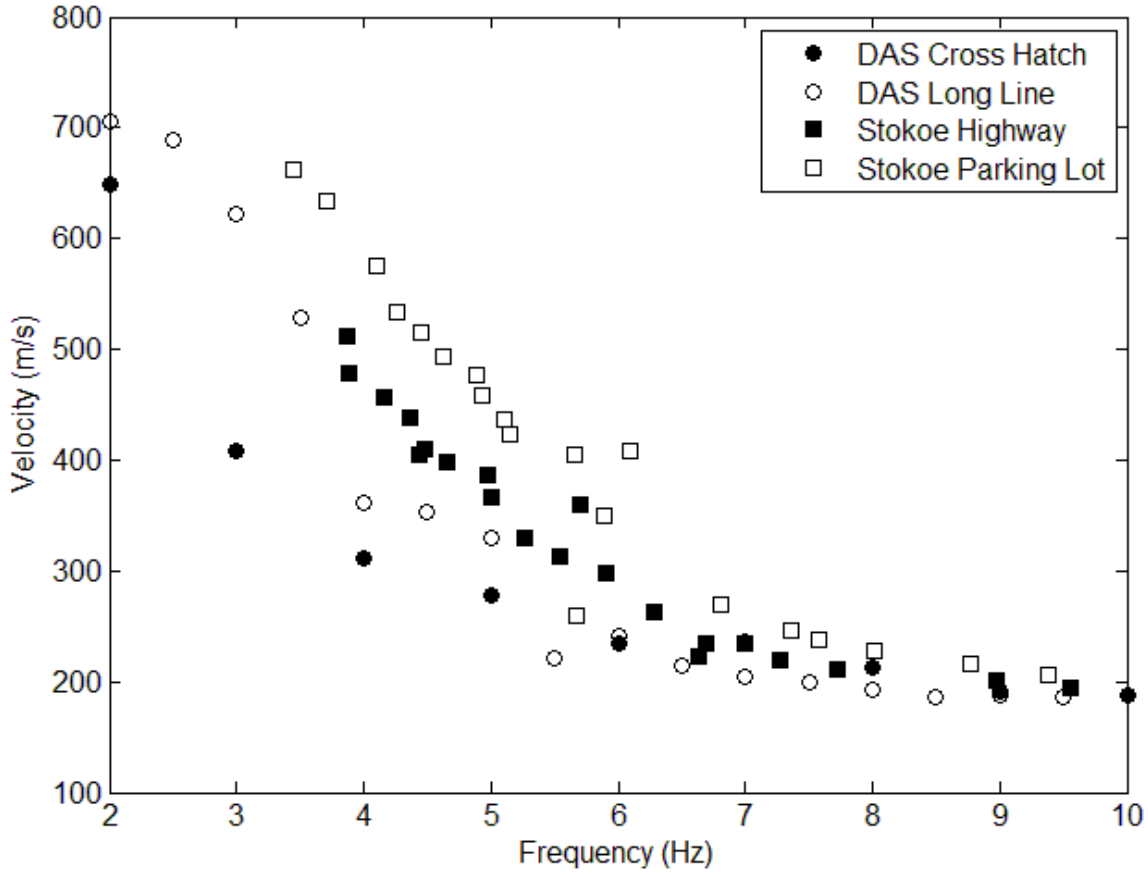

Figure 2.8: Dispersion curve results from both DAS lines along with results from the two lines in the study by Stokoe et al. (2004). The parking lot line had variable results due to poorly-graded gravel, so the highway line is used for comparison.

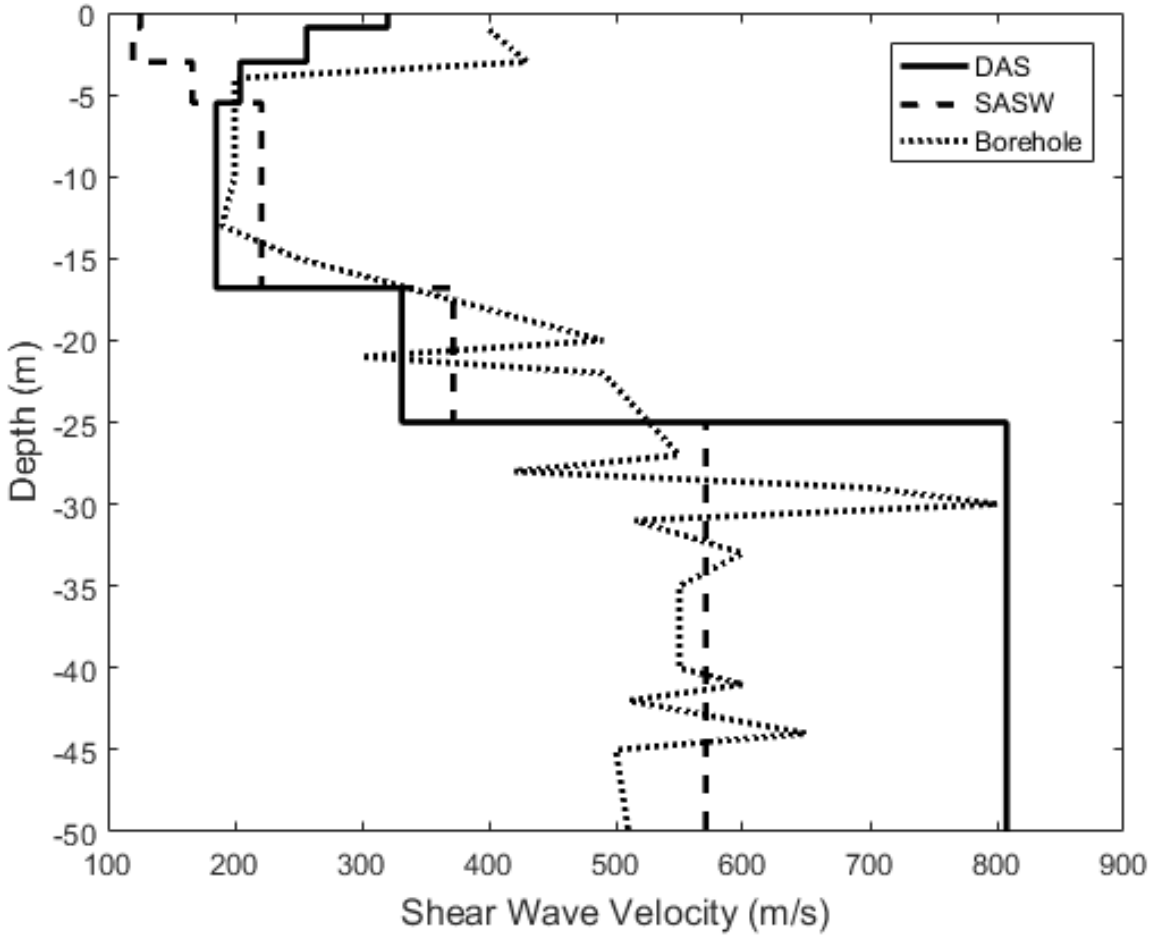

Figure 2.9: Shear-wave velocity profile inverted from dispersion curves from the DAS long line as well as previous result by Stokoe et al. (2004) and borehole geophysical logs from Steller (1996).

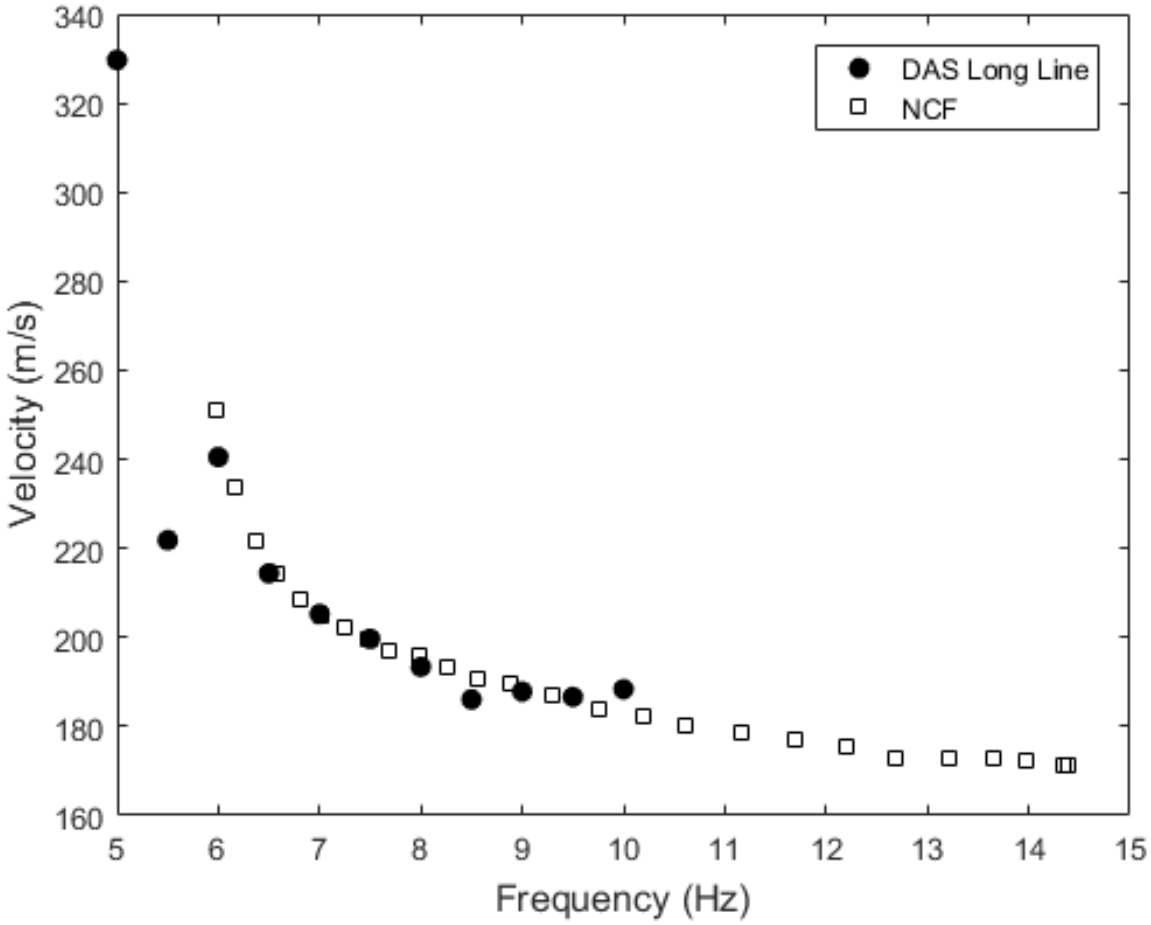

Figure 2.10: Dispersion curves from the DAS long-line active source traces (solid circles) and the NCF passive source result (open squares) (Zeng et al., 2016).

Tables

Table 2.1: Parameters used in SWAMI Inversion

Top of Layer Depth (m)	Layer Thickness (m)	P-Wave Velocity (m/s)	S-Wave Velocity (m/s)	Poisson's Ratio	Density (kg/m^3)
0	0.9	256.6	137.2	0.3	1762
0.9	2.1	421.9	225.5	0.3	1762
3.0	2.4	1524	161.5	0.49	2002
5.4	11.3	1524	211.8	0.49	2002
16.7	8.2	1524	268.2	0.48	2002
24.9	Halfspace	1524	518.1	0.43	2002

Chapter 3

Travel-Time Tomographic Imaging using Distributed Acoustic Sensing (DAS)

Introduction

Subsurface imaging using seismic waves is applied to energy, environmental, and engineering problems. Seismic images obtained from travel-time data are improved by a greater number of rays passing through the imaged volume. Distributed Acoustic Sensing (DAS) contains the potential for high-spatial density of stations combined with large spatial sizes. In DAS an interrogator sends a laser pulse into the cable. Rayleigh backscattering of light occurs throughout the cable as a result of minor defects in the silica. A characteristic signature of reflections over a short segment of fiber (the gauge length) can be used to monitor its change in length between two successive laser pulses (Parker et al. 2014; Daley et al. 2015). The gauge length is the spatial resolution and it is typically on the order of 10 meters. The center of the gauge length is called a channel, and the strain rate over the gauge length is labeled by the location at its center. DAS allows for a sampling resolution of a channel every meter, meaning a measurement of strain rate can be calculated every meter for distances up to 100 km and at sampling rates of as fast as 100 kHz (Johannessen et al. 2012; Miller et al. 2012). The ability to sense long cable lengths means that relatively large areas or volumes can be enclosed either for locating events within the surrounded area or volume or for obtaining tomographic images.

To date, DAS has been applied largely for characterizing hydrocarbon reservoirs and monitoring carbon sequestration sites using Vertical Seismic Profiling (VSP). For example, Miller et al. (2012) placed fiber-optic cable into a well and along the ground surface at the

University of Texas' EGL Devine Test Site near San Antonio, Texas. The stratigraphy in the well was known from previous characterization studies. A Vibroseis source occupied four locations on the surface. The DAS data were of similar quality to traditional borehole seismic tools.

Madsen et al. (2013) used DAS on previously-installed fiber-optic cables in three producing wells in the North Sea simply by connecting four DAS units to the ends of the fibers. Two of the three wells had multiple cables, which were used to compare the response in two different cables at approximately the same location. Shots were gathered from a seismic source vessel. Madsen et al. found that the separate cables showed good agreement at the same location and the quality of the data would lend itself well to VSP.

A significant practical attribute of DAS is that cable can be permanently cemented behind casing to provide a complete set of sensors over the entire length of the well for repeat VSPs without having to reoccupy the well with a string or provide power to geophones. In addition, a survey can be completed without having to move a string of geophones to various levels within the well. Daley et al. (2015) used DAS in a well for a CO_2 storage monitoring pilot in Alabama. The DAS array and co-located geophones were excited using a Vibroseis truck and were used for VSP. They found that the DAS array data matched that of the geophones in both phase and amplitude.

Installing DAS at the surface requires coupling the cable to the sensed medium. Castongia et al. (2016) conducted a two-dimensional tomography study of lake ice by freezing in a triangular array (30 meters on a side) of fiber-optic cable on the surface of Lake Mendota in Madison, Wisconsin. A sledgehammer was used as a source and an Akaike Information Criterion (AIC) picker was used to pick first arrivals. A 2D tomogram of ice velocity was

created using source locations both inside and outside the array. Overall, the velocities determined were within the expected range for thin ice and they showed subtle variations associated with thickness.

The present study is based on a rectangular, 762-meter DAS array at Garner Valley, California. The fiber-optic cable was buried about 0.3 m below the surface by trenching and backfilling. A variety of sources were deployed, including a swept-frequency, large, shear-shaker in a fixed location outside the array, a Vibroseis truck, a portable shear-shaker, and hammer blows. The large shear-shaker was used to obtain subsurface profiles of shear-wave velocity using the technique of Multispectral Analysis of Surface Waves (MASW) (Lancelle et al., 2016 submitted). Traffic noise on a highway that paralleled one leg of the array was used as an ambient noise source to obtain nearly identical results (Zeng et al., 2016).

In the study presented in this paper the Garner Valley array was used to obtain a two-dimensional image of the refracting layer below the water table from the first arrival and the refracted arrival. The goal was to determine the resolution that can be achieved using a DAS array where the density of sensors is much larger than the density that is typically achieved with geophone arrays. The organization of the paper is first to describe the study site followed by details of the methodology of selecting arrivals and obtaining travel times. Then the inversion method is presented followed by the resulting images at different nodal separations. The discussion centers around the resolution that is appropriate for the images and special considerations when using DAS.

Tomographic Studies

Near surface refraction tomography has been used in a number of studies for a variety of different uses. Lanz et al. (1998) used first-arrival traveltime tomography to image landfills in Switzerland. They wanted to determine the depth and geometry of the lower boundary of the landfill. The tomographic refraction scheme was found to be efficient to study the shallow subsurface, but other geological or geophysical data were needed to distinguish velocity anomalies associated with the landfill from velocity anomalies associated with natural variations in geology.

Samyn et al. (2012) used first-arrival traveltime tomography to create a 3D high-resolution image of landslide areas in order to improve early warning. They were successfully able to image the boundary between the landslide and the surrounding stable slopes as well as the structures within the landslide at a small scale. Their results compared well with borehole results and a 2D refraction seismic survey.

Zelt et al. (2006) used 3D refraction data at Hill Air Force Base, Utah in a 95 m by 40 m area to image a groundwater contamination site some 20 m in depth. They wanted to test the ability of 3D first-arrival time data to characterize the shallow environment for use in remediation of the site. Their 3D velocity model compared well with two other models from the site, although the velocity model was likely a smoothed version of the actual model due to the size of the Fresnel zone.

Zhang and Toksöz (1998) conducted a near surface refracted study to image a coastal site in Boston, Massachusetts. They used two lines of 24 geophones to image the subsurface beneath a tidal plain in order to locate an area of deeper bedrock for construction purposes. Their inversion used an improved shortest path raytracing algorithm they developed as well as

Tikhonov regularization. Their subsurface image corresponded well with results obtained from boreholes.

Each of the previously mentioned studies used refracted waves to image a near-surface site. In all cases the resolution of the tomographic images was important to understanding the images. Refraction tomography is used in this study to help assess the applicability of DAS seismic data to near-surface geophysical imaging and to determine a proper resolution for this array.

Study Area

In September 2013 a set of elastic wave experiments were conducted at the George E. Brown Jr. Network for Earthquake Engineering Simulation field site in Southern California (http://nees.ucsb.edu/facilities/GVDA) Garner Valley Downhole Array (GVDA). The GVDA, which is operated by the University of California Santa Barbara, is located 20 km southwest of Palm Springs, California. The site is in a seismically active region 7 km east of the San Jacinto fault and 35 km west of the San Andreas fault. The near-surface geology of the site has been fully characterized with both geophysical studies (e.g., Stokoe et al. 2004) and geotechnical engineering studies (Youd et al. 2004) and is shown in Figure 3.1. From the surface to about 18 m depth, the subsurface is composed mostly of flat-lying silty and sandy soil. Below that is a 7 m transition between the silty, sandy soil and the underlying decomposed granite. The weathered, decomposed granite continues to a depth of about 88 meters, and that is underlain by granite bedrock. The sediments at the site are mostly homogeneous throughout the area. Steller (1996) performed geophysical borehole studies at the site and the P-wave velocity log is plotted in Figure 3.2. P-wave velocities at the surface were measured to be about 400 m/s and at

approximately 5-m depth the velocity was about 1600 m/s. At 20-m depth the velocity rose to an average of 2000 m/s and maintained that average velocity until the contact with the bedrock. Water table depth varies throughout the seasons between as shallow as 1 m and as deep as 6 m. For the refracted-wave tomography at Garner Valley, the water table is expected to be an important refractor. The experiments at the GVDA field site were conducted to evaluate the applicability of DAS as a high density seismic array for near surface geophysical exploration.

A 762-meter-long Optical Cable Corporation fiber-optic cable was trenched into a rectangular array with two sub-diagonals (Figure 3.3) at a depth of about 0.3 m. The perimeter of the array is approximately 160 m by 80 m. After trenching the cable was covered with soil to provide coupling between the cable and the ground. The fiber-optic cable included two single-mode and two multi-mode tightly-buffered fibers in the same jacket. The single-mode fibers were used in the DAS configuration. They were spliced together at the end of the line to allow for two co-located measurements along the whole length of the fiber.

Tomographic Inversion Analysis

We used travel time data from two different seismic sources to obtain 2D tomographic images of a refracting layer. A small hammer hitting a plate generated signals only traveling near the surface of the testing site and was used to determine a near-surface velocity. The hammer impacts were originally intended to identify specific locations along the DAS cable and were placed at all corners of the array as well as at a few other locations along the fiber. A metal plate was placed and struck at 13 surveyed locations around the array. Multiple hammer blows were repeated at each location. The raw data traces from every tenth channel were used to pick first arrivals. Multiple traces were not stacked, so all manual travel-time picks were made from a

single hammer blow from each shot location. The gauge length used in this study was 10 m, so every tenth channel was chosen to make each DAS measurement independent. The arrival times were plotted against shortest-path distances and outliers were removed. The average velocity for the surface sediments was found to be 250 m/s, shown in Figure 3.4.

The tomographic analysis used in this study utilized refracted waves arrivals from Vibroseis truck sweeps. The 27-kN vertical-shaking Vibroseis truck was supplied and operated by GeoVision, and occupied 8 different locations around the array (Figure 3.3). The Vibroseis truck created a linear sweep over frequencies from 20 to 100 Hz over 10 seconds. All sweeps were repeated 10 times at each location. Multiple processing steps were used to prepare the Vibroseis sweeps for manual picking of the refracted arrival and are shown in Figure 3.5. First, an idealized linear Vibroseis sweep from 20 to 100 Hz over 10 seconds was used to pre-process the force sensor at the foot of the truck using a source synchronous filter (SSF) described by Lord et al. (2016). Each received DAS channel was source delay filtered (SDF) to follow the same frequencies as the source was outputting. SDF is the same as SSF but allows for travel-time between the source and the receiver. Then the filtered truck sweep was cross-correlated with the filtered DAS waveform and all 10 cross-correlated sweeps were stacked to obtain the waveform that was used for the arrival picking. An algorithm was developed to help the user interactively pick the refracted arrival in the stacked cross-correlations (Lord et al. 2016). The linear moveout, static delay, and bandpass filter can all be adjusted interactively on a computer screen to align the wave arrival with a horizontal cursor line (Figure 3.6). The bandpass filter allows for separation of the high-frequency refracted arrival from the relatively lower frequency direct waves. Once coherent arrivals are found, picks for individual traces can be made. Picks in this study had a timing uncertainty of 10 milliseconds. Straight ray-paths for each arrival are

plotted in Figure 3.7 and the travel times are plotted against straight-ray path length (Figure 3.8). The refracting layer in this study is assumed to be the water table. The average velocity of the refracting layer was found to be 1850 m/s. The depth to the refractor, in this case the water table, was also calculated and was found to be approximately 4.5 meters using the top layer velocity of 250 m/s calculated from the hammer blow data.

In order to prepare the picks for input into the 2-D inversion code the sources and receivers needed to be relocated on the refractor. The process of doing so is shown in Figure 3.9. The surface layer was assumed to have a velocity of 250 m/s, from the direct arrival analysis, and the refractor is assumed to have a velocity of 1850 m/s. Since the surface is relatively flat, the saturated refractor was also assumed to be flat and at a depth of 4.5 meters.

The code used in this study for the 2-D inversion is called PRONTO (Aldridge and Oldenburg 1993). Two key features of PRONTO are (i) use of a finite difference algorithm for rapid forward modeling of traveltimes, (ii) inclusion of constraint information in order to restrict the nonuniqueness, and smoothing of the results using regularization schemes (Aldridge and Oldenburg 1993). PRONTO was developed to invert for velocity fields in 2D systems. The inversion procedure is completed in four basic steps: 1) calculation of arrival times, 2) generation of curved raypaths between all source-receiver pairs, 3) solution of the system of linear equations for a perturbation to the existing slowness model, and 4) updating and optionally smoothing the slowness model. These four steps are repeated until the root-mean-square traveltime residual is acceptable or the maximum number of iterations is reached. The reciprocal of the slowness model is then the final velocity model.

PRONTO is not restricted to any specific source-receiver setup so it could be used in VSP surveys as well as in setups like the one in this study. It can also incorporate topography.

While removal of outliers can be done ahead of time, PRONTO does have an option to set a lower and upper bound to the pick times and it will remove any times below or above those limits. PRONTO also has the ability to apply constraints to the slowness model to stabilize the inversion and incorporate geological knowledge (Aldridge and Oldenburg 1993). Because PRONTO is flexible in both source-receiver locations and allows for constraints to be applied to the model, it was chosen for use in this study.

For the refracted-wave tomography, the projected locations of the sources and receivers were used as well as the travel time along the refractor. It was assumed the surface and refractor layers were perfectly horizontal.

Results

A 2D tomographic inversion was completed for refracted arrivals. All 8 Vibroseis truck locations were used and a total of 995 arrival times out of a possible 3737 were used for the inversion. Raypaths for those arrival times are shown in Figure 3.7. Approximately every fourth DAS channel was used. Since the locations of the sources and receivers were relocated to the refracting layer, there were a total of 995 relocated source locations used in the inversion. PRONTO limits the number of source locations to 1000. The inverted velocity field and information content is plotted in Figure 3.10 for three nodal separation sizes: 20 m by 20 m, 10 m by 10 m, and 5 m by 5 m. The information content gives the sum of the length of the rays passing through each nodal dimension divided by the nodal separation. The higher the information content the more rays there were passing through that block representing the nodal separation. Since the study area is fairly homogeneous at the surface, we expect the inverted velocity field to also be relatively homogeneous.

The initial-guess straight raypaths used for refracted-wave tomography are given in Figure 3.7. Although DAS generally is not sensitive to orthogonal particle motion, many rays were at a high angle to the cable and time arrival was still able to be successfully picked due to the higher energy of the source and the pre-processing of the data.

Figure 3.10 shows the inverted velocity field for three nodal separation sizes. P-wave velocities are given in m/s and the information content is a dimensionless quantity that represents the total ray length per nodal separation divided by the nodal separation. For the 20 m by 20 m nodal separation, the majority of the center of the array has good ray coverage according to the information content. The average velocity for this nodal separation is 2051 m/s, and the residual is 1.1×10^{-4} s. This is about 200 m/s above the average velocity expected from straight ray paths. For the 10 m by 10 m nodal separation the ray coverage is still fairly strong within the array, though there are a few boxes with almost no ray coverage towards the edges of the array. The average velocity for this nodal separation is 2031 m/s and the residual is 9.0×10^{-5} s. Velocity inversion results from the 5 m by 5 m nodal separation appear to be more poorly constrained based on the information content. While the residual value of 8.7×10^{-5} s is the lowest of the three, there are many boxes that do not contain any rays traveling through them and the lower residual likely represents fitting the noise rather than the actual signal. Thus, the 5 m by 5 m nodal separation is not reliable for determining velocity structure.

Discussion

Influence of Particle Motion-Cable Direction Angle

Particle motions orthogonal to the fiber-optic cable will not be picked up by the DAS system, as the cable is sensitive to axial strain. Mateeva el al. (2014) show the DAS response

when particle motions are perpendicular to the longitudinal axis of the optical fiber. Figure 3.11 shows an example of the directional sensitivity of DAS in this array. Received DAS data are plotted for one hammer blow both in line with the source and approximately perpendicular to the source. There is a drop-off in amplitude in the DAS channels perpendicular to the source relative to those in line with the source. However, it is important to note that even at high angles to the particle motion, the fiber-optic cable shows some response for high-energy excitations.

While the fiber response to orthogonal particle motion is a limitation inherent to the DAS system, there are ways to work around it. Adding zig-zags in the cable layout would lead to shorter segments of cable that are perpendicular to the incoming waves. Another option for overcoming the DAS directional sensitivity limitation is to use specialty fiber, as presented by Hornman (2016). Hornman used a helically wound cable which was designed to have broadside sensitivity in order to use cable as the sensing element in reflection seismology. The helically wound cable was placed in a shallow horizontal borehole along with a hydrophone streamer and was tested using an accelerated weight drop. Hornman found that the helically wound cable successfully recorded broadside waves. To add flexibility in the interpretation of seismic studies the use of helically wound cable would provide a good alternative to a standard fiber-optic cable.

Comparison with Shear-Wave Profile Results

Lancelle et al. (2016) completed a study using the same DAS array but for a large shear-shaker source to create dispersion curves and shear-wave velocity profiles along lines of the cable (Figure 3.12). The Multispectral Analysis of Surface Waves (MASW) study encompassed a depth range greater than the two layers of this study, but a general comparison can be made. The shear velocity can be estimated from the first-arrival P-wave velocity from the Poisson's ratio of 0.3 assumed in the MASW study. Using that Poisson's ratio and the average 250 m/s P-

wave velocity found from the hammer blows, an expected shear-wave velocity at the surface would be about 134 m/s. In the shear-wave velocity profile from the Lancelle study the velocity at the surface calculated from the DAS array was about 320 m/s and just below the surface the velocity dropped to about 200 m/s (Figure 3.12). The reason for this difference could be due to the inversion from the wavelengths used in the Lancelle study. The shortest wavelength used in the shear wave velocity profile inversion was approximately 18 m, meaning the velocity is an average over 18 m of depth, not focused at the surface as the velocity from the hammer blows is. The refracted-wave tomographic image could be used to better constrain the velocity structure near the surface and the shear-wave velocity profile produced by MASW could be used to better understand what the velocity structure is at greater depth, creating a 3-D picture of the velocity structure in the subsurface.

Pasquet et al. (2015) used P-wave refraction tomography and surface wave dispersion analysis to estimate a Vp/Vs ratio. They found that the Vs profile determined from surface waves correctly matched the general features of a Vs profile determined by SH waves and that if the Vs profile from surface waves was characterized by strong velocity uncertainties in the deepest layers that the profile provided a more detailed look at the lateral variations in the shallow layers. They found that calculating a Vp/Vs ratio from the surface-wave Vs profile showed higher lateral resolution and matched the features found using electrical resistivity tomography so the approach of using surface waves in combination with P-wave refraction was successful. In future studies, a combination of near-surface 2D tomography and MASW could create a better understanding of changes in velocity, both laterally and with depth.

Conclusions

A 762-meter-long DAS array was used in a field trial in Southern California to test the suitability of DAS for near surface tomographic studies. Tomographic inversions were successfully completed for refracted arrivals. The resolution of the DAS array could be as small as 10 m by 10 m, though 5 m by 5 m was too small since there were many boxes within the study area that had no rays passing through them. The directional sensitivity of DAS needs to be considered when completing tomographic studies. Particle motion arriving orthogonal to the fiber will not be measured, so planning of a DAS array and the orientation of the fiber with respect to expected particle motion is important to the success of a future DAS study.

References

Aldridge D., and Oldenburg D. 1993. Two-Dimensional Tomographic Inversion with Finite-Difference Traveltimes, Journal of Seismic Exploration, 2, 257-274.

Castongia E., Wang H. F., Lord N., Fratta D., Mondanos M., and Chalari A. 2016. An Experimental Investigation of Distributed Acoustic Sensing (DAS) on Lake Ice, *Journal of Environmental and Engineering Geophysics* (under review).

Daley T. M., Miller D. E., Dodds K., Cook P., and Freifeld B. M. 2015. Field testing of modular borehole monitoring with simultaneous distributed acoustic sensing and geophone vertical seismic profiles at Citronelle, Alabama, *Geophysical Prospecting*, Article first published online: 2 Nov. 2015, doi: 10.1111/1365-2478.12324.

Hornman J.C. 2016. Field trial of seismic recording using distributed acoustic sensing with broadside sensitive fibre-optic cables, *Geophysical Prospecting*. doi: 10.1111/1365-2478.12358

Johannessen K., Drakeley B., and Farhadiroushan M. 2012. Distributed Acoustic Sensing - a new way of listening to your well/reservoir, *SPE Intelligent Energy International* held in Utrecht, The Netherlands, 27–29 March 2012, SPE 149602, 9 pp.

Lancelle C., Baldwin J., Lord N., Fratta D., Chalari A., Wang H. F. 2016. Using Distributed Acoustic Sensing (DAS) for Multichannel Analysis of Surface Waves (MASW) to Evaluate Ground Stiffness, *Near Surface Geophysics* (under review).

Lanz E., Maurer H., and Green A. 1998. Refraction Tomography over a Buried Waste Disposal Site, *Geophysics*, 63(4), 1414-1433.

Lord N., Wang H. F., and Fratta D. 2016. A Source-Synchronous Filter for Uncorrelated Receiver Traces from a Swept-Frequency Seismic Source, *Geophysics* (in press).

Madsen K.N., Dümmong S., Kritski A., Pedersen Å.S., Finfer D., Gillies A., and Travis P. 2013. Simultaneous Multiwell VSP in the North Sea Using Distributed Acoustic Sensing, 75th EAGE Conference & Exhibition incorporating SPE EUROPEC 2013, London, UK, 10-13 June 2013, 5 pp.

Mateeva A., Lopez J., Potters H., Mestayer J., Cox B., Kiyashchenko D., Wills P., Grandi S., Hornman K., Kuvshinov B., Berlang W., Yang Z., and Detomo R. 2014. Distributed acoustic sensing for reservoir monitoring with vertical seismic profiling, *Geophysical Prospecting*, 62, 679–692, doi: 10.1111/1365-2478.12116.

Miller D., Parker T., Kashikar S., Todorov M., and Bostick T. 2012. Vertical Seismic Profiling using a fibre-optic cable as a Distributed Acoustic Sensor, 74th EAGE Conference & Exhibition incorporating SPE EUROPEC 2012, Copenhagen, Denmark, 4-7 June 2012, 5 pp.

Parker T., Shatalin S. V., and Farhadiroushan M. 2014. Distributed Acoustic Sensing - A new tool for seismic applications. *First Break*, February 2014, 61-69.

Pasquet S., Bodet L., Longuevergne L., Dhemaied A., Camerlynck C., Rejiba F., and Guérin R. 2015. 2D Characterization of Near-Surface V_P/V_S: surface-wave dispersion inversion versus refraction tomography, *Near Surface Geophysics*, 13, 315-331.

Samyn K., Travelletti J., Bitri A., Grandjean G., and Malet J.-P. 2012. Characterization of a Landslide Geometry using 3D Seismic Refraction Traveltime Tomography: The La Valette Landslide Case History, *Journal of Applied Geophysics*, 86, 120-132.

Steller R. 1996. *New Borehole Geophysical Results at GVDA*, Data Report.URL: http://nees.ucsb.edu/sites/eot-dev.nees.ucsb.edu/files/facilities/docs/GVDA-Geotech-Stellar1996.pdf [Accessed on June 9, 2016].

Stokoe K. H., Kurtulus A., and Menq F.-Y. 2004. *Data Report: SASW Measurements at the NEES Garner Valley Test Site, California*, 13 January 2004, 12 pp.

Youd T. L., Bartholomew H. A. J., and Proctor J. S. 2004. *Geotechnical logs and data from permanently instrumented field sites: Garner Valley Downhole Array (GVDA) and Wildlife Liquefaction Array (WLA)*, Data Report.URL: http://nees.ucsb.edu/sites/eot-dev.nees.ucsb.edu/files/facilities/docs/geotech-data-report.pdf [Accessed on January 9, 2016].

Zelt C., Azaria A., and Levander A. 2006. 3D Seismic Refraction Traveltime Tomography at a Groundwater Contamination Site, *Geophysics*, 71(5), H67-H78.

Zeng X., Lancelle C., Thurber C., Fratta D., Wang H. F., Lord N., Chalari A., and Clarke A. 2016. Properties of Noise Cross-correlation Functions Obtained from a Distributed

Acoustic Sensing Array at Garner Valley, California, *Bulletin of the Seismological Society of America* (under review).

Zhang J. and Toksöz M. N. 1998. Nonlinear Refraction Traveltime Tomography, *Geophysics*, 63(5), 1726-1737.

Figures

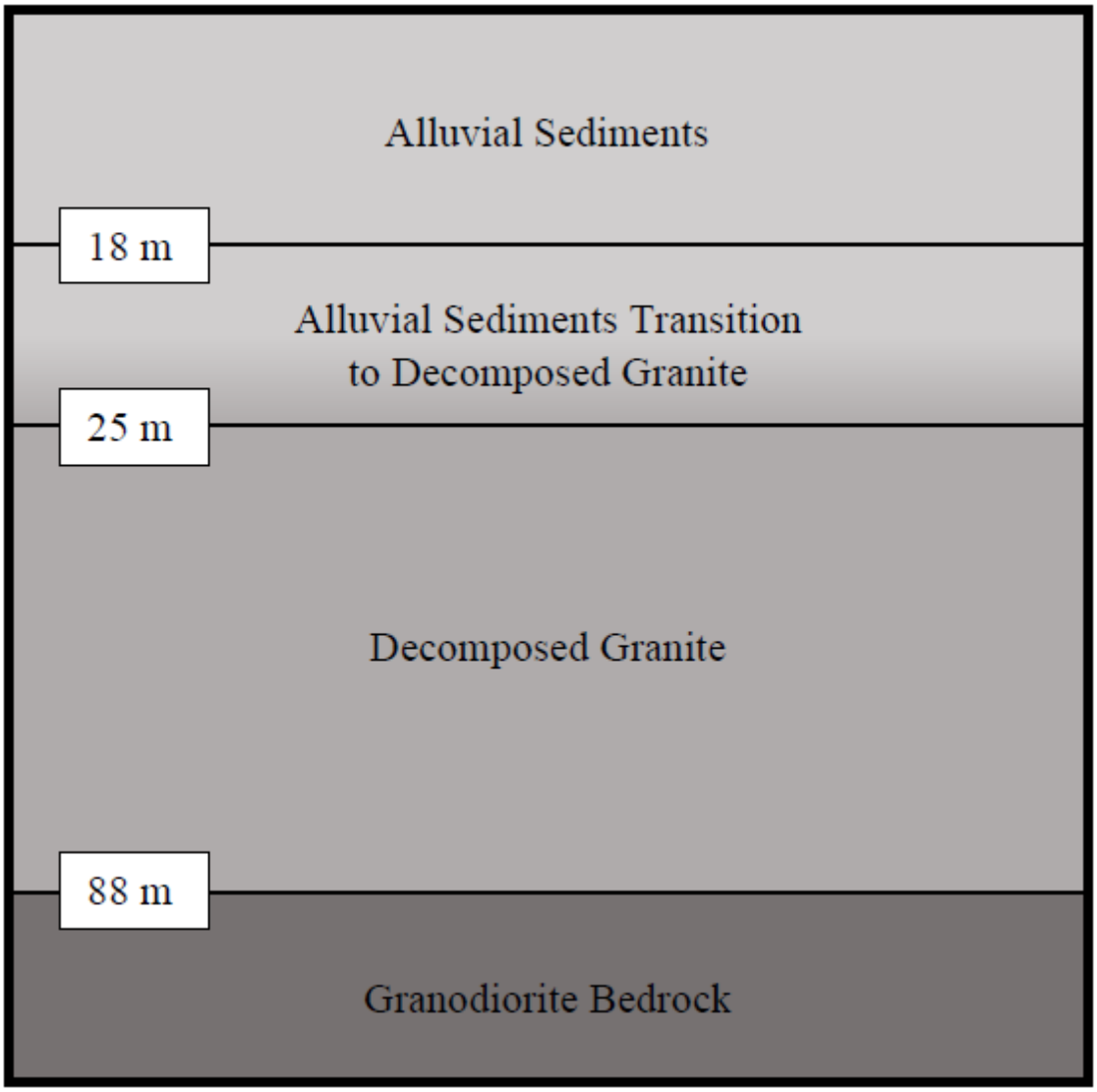

Figure 3.1: Stratigraphic cross-section of the study area.

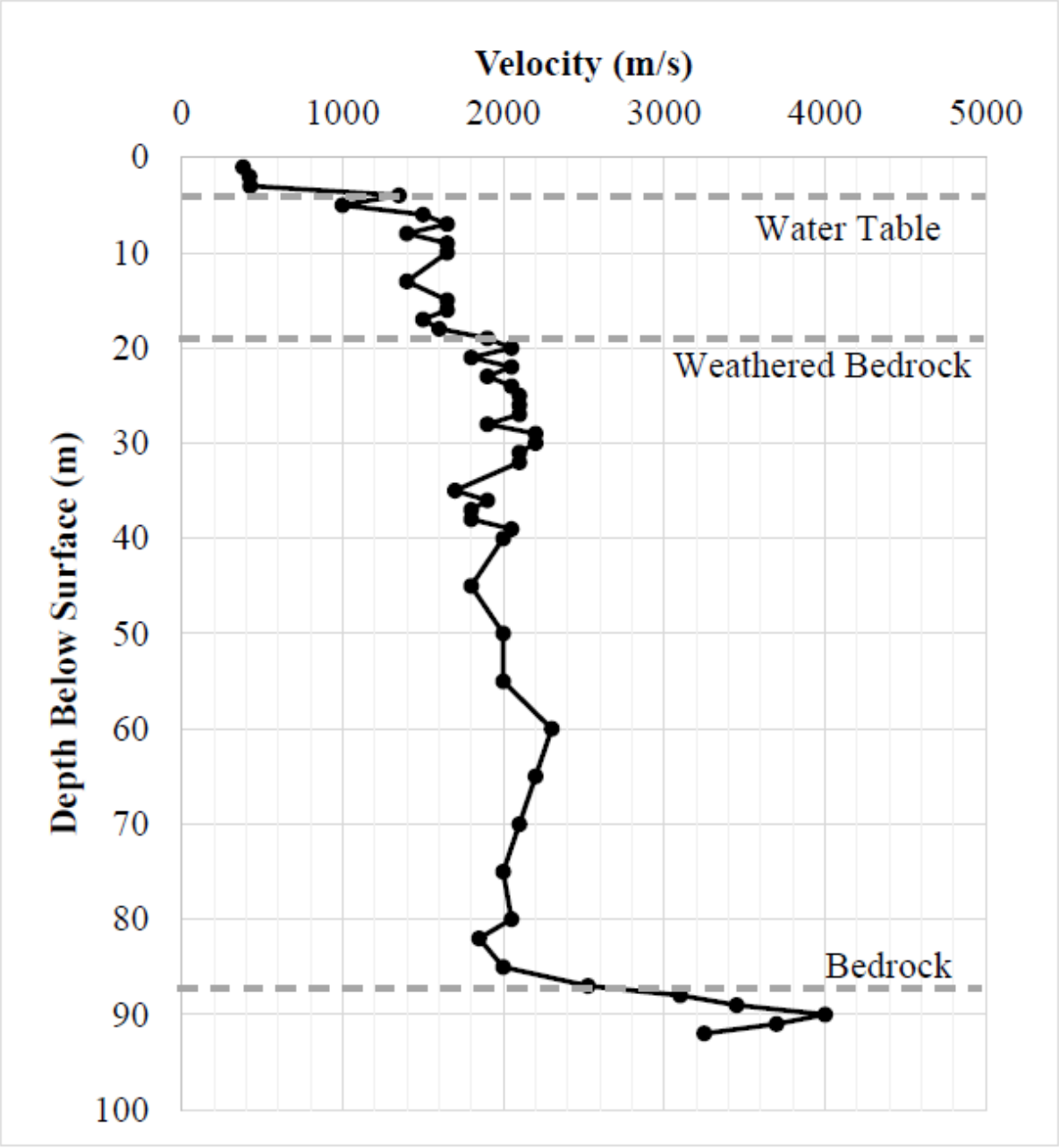

Figure 3.2: P-wave geotechnical log from Steller (1996). Water table is between 5 and 8-m depth; weathered bedrock at about 20-m depth, and contact with bedrock occurs at 88 m depth.

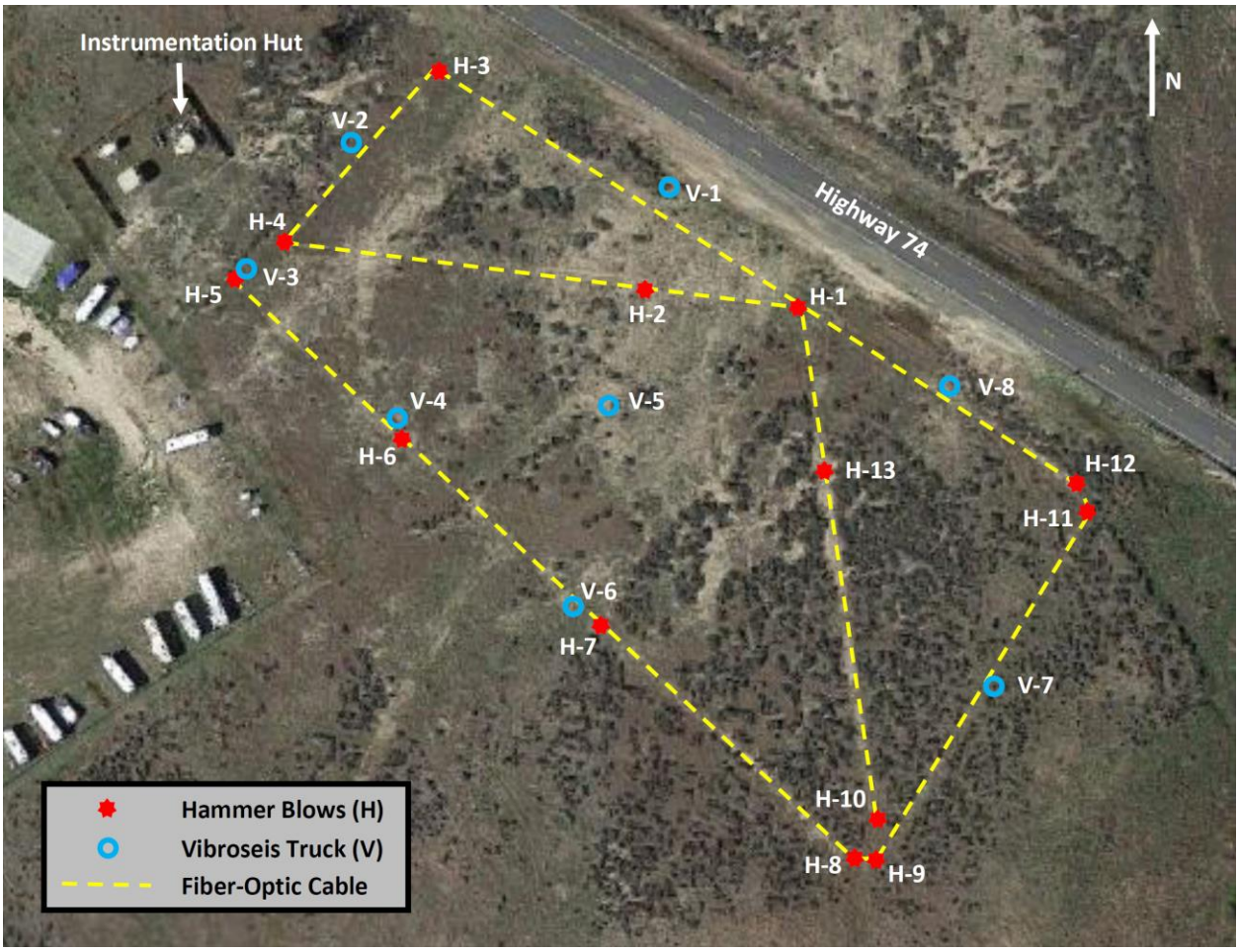

Figure 3.3: Map of Garner Valley study area with layout of DAS cable denoted by yellow dashed line, hammer blows marked by red and Vibroseis truck locations marked by blue.

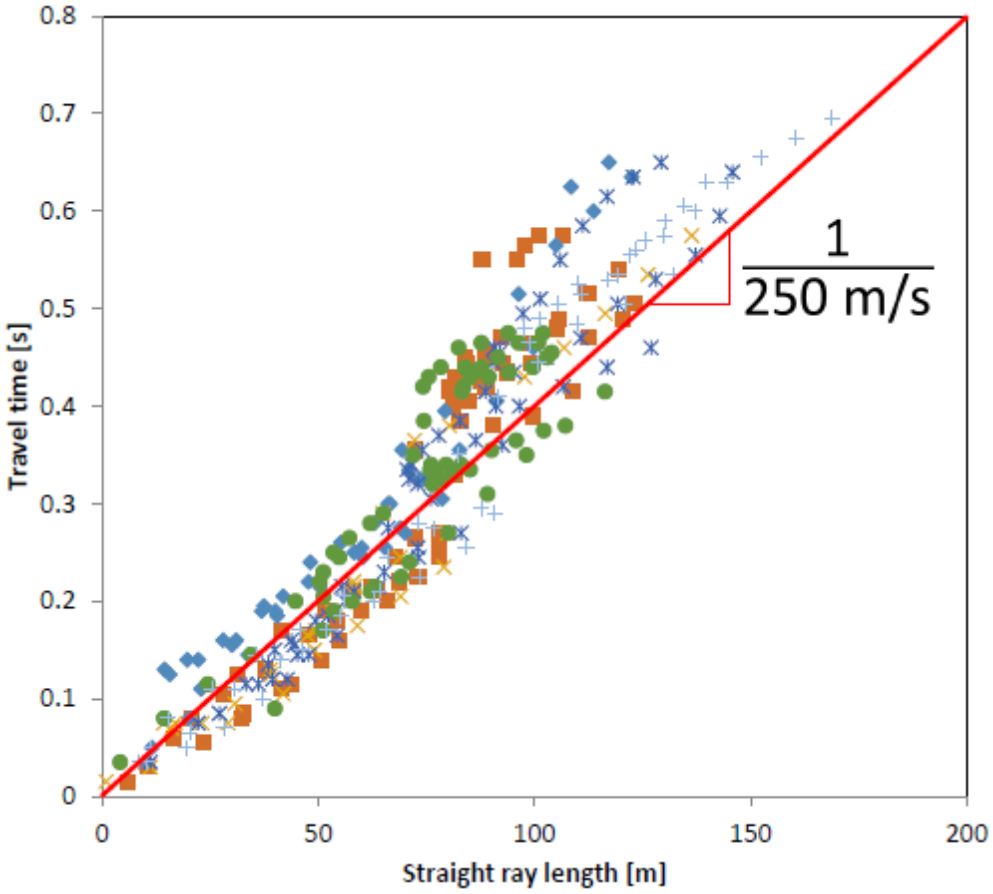

Figure 3.4: Plot of all first arrival times against the straight line distance between source and receiver. The average velocity is 250 m/s. Each point represents one arrival time and each different symbol represents a different source.

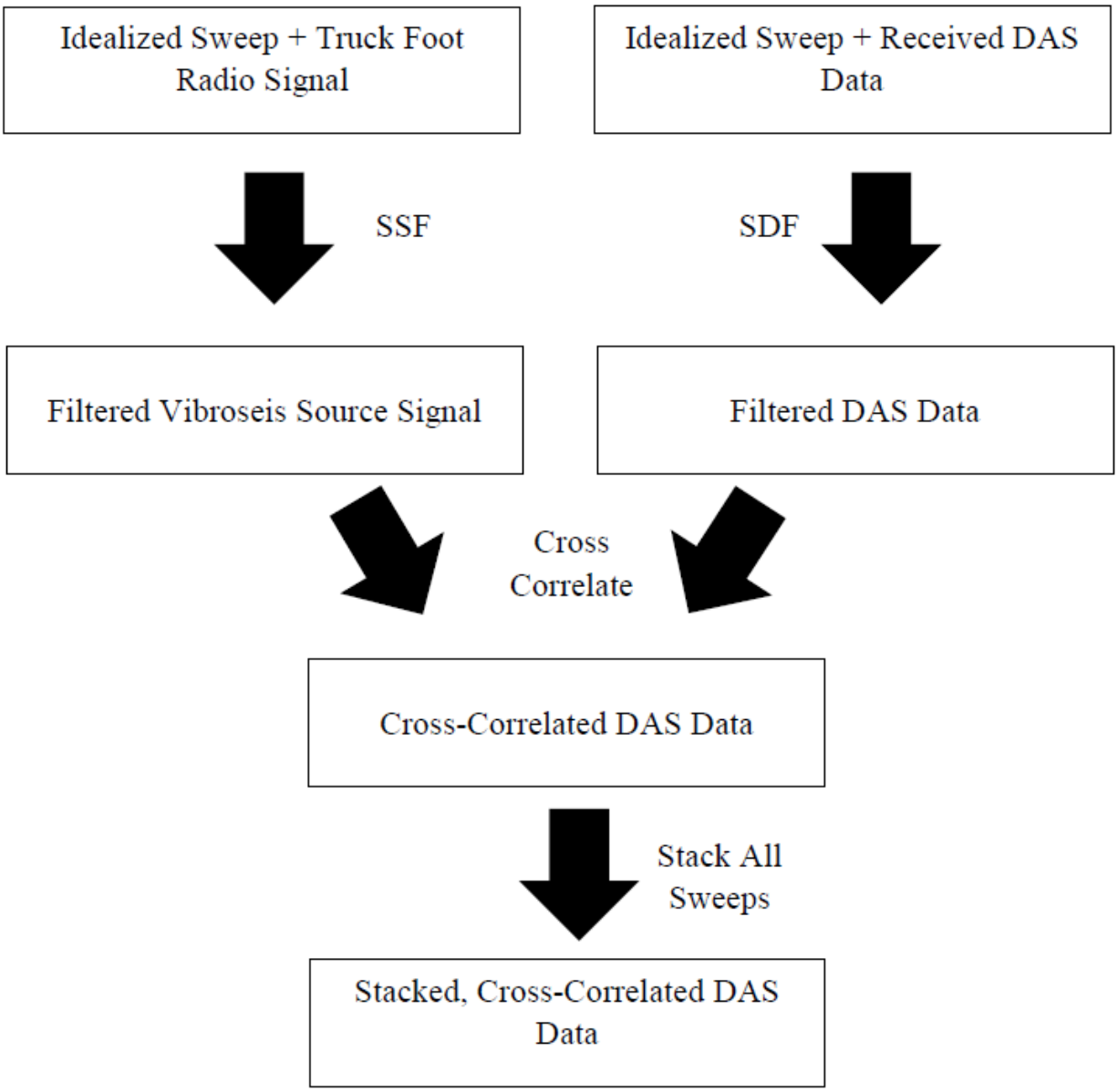

Figure 3.5: Flowchart of data processing for Vibroseis sweeps.

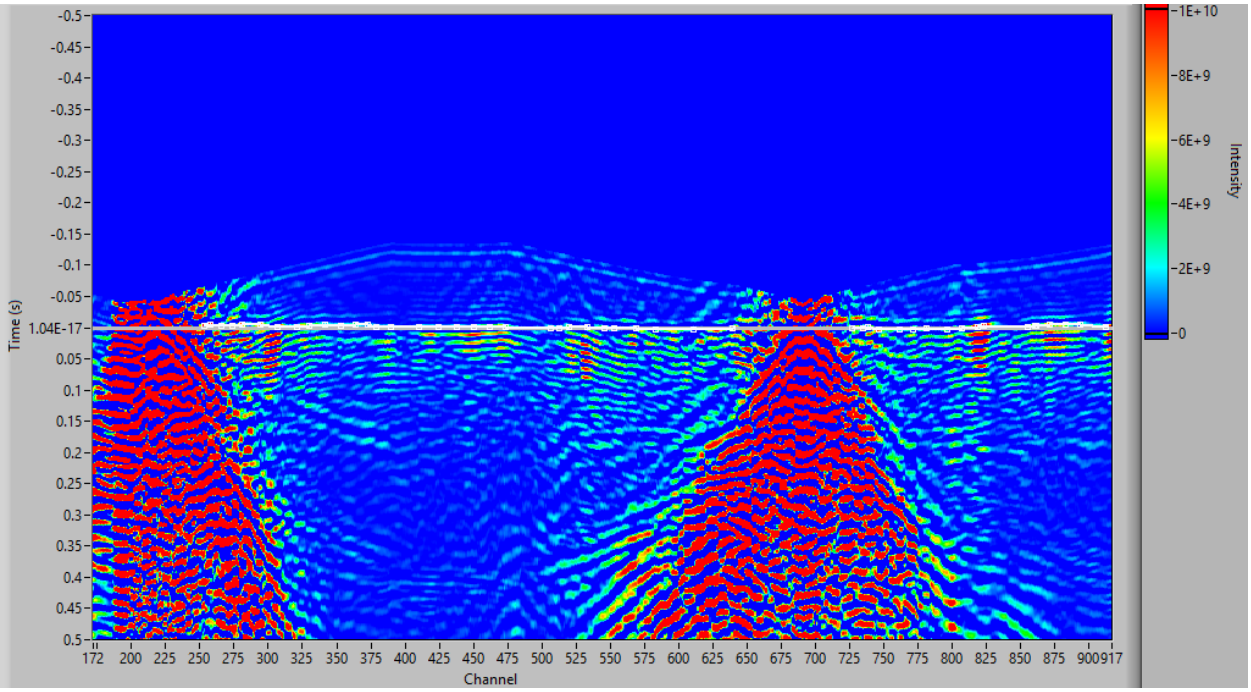

Figure 3.6: Image of Phase Analysis Tool with the moveout velocity adjusted so that the refracted arrival appears flat and lies along the grey reference line. Picks are shown as white squares along that reference line. The strongest refracted arrival seen across the entire array was picked.

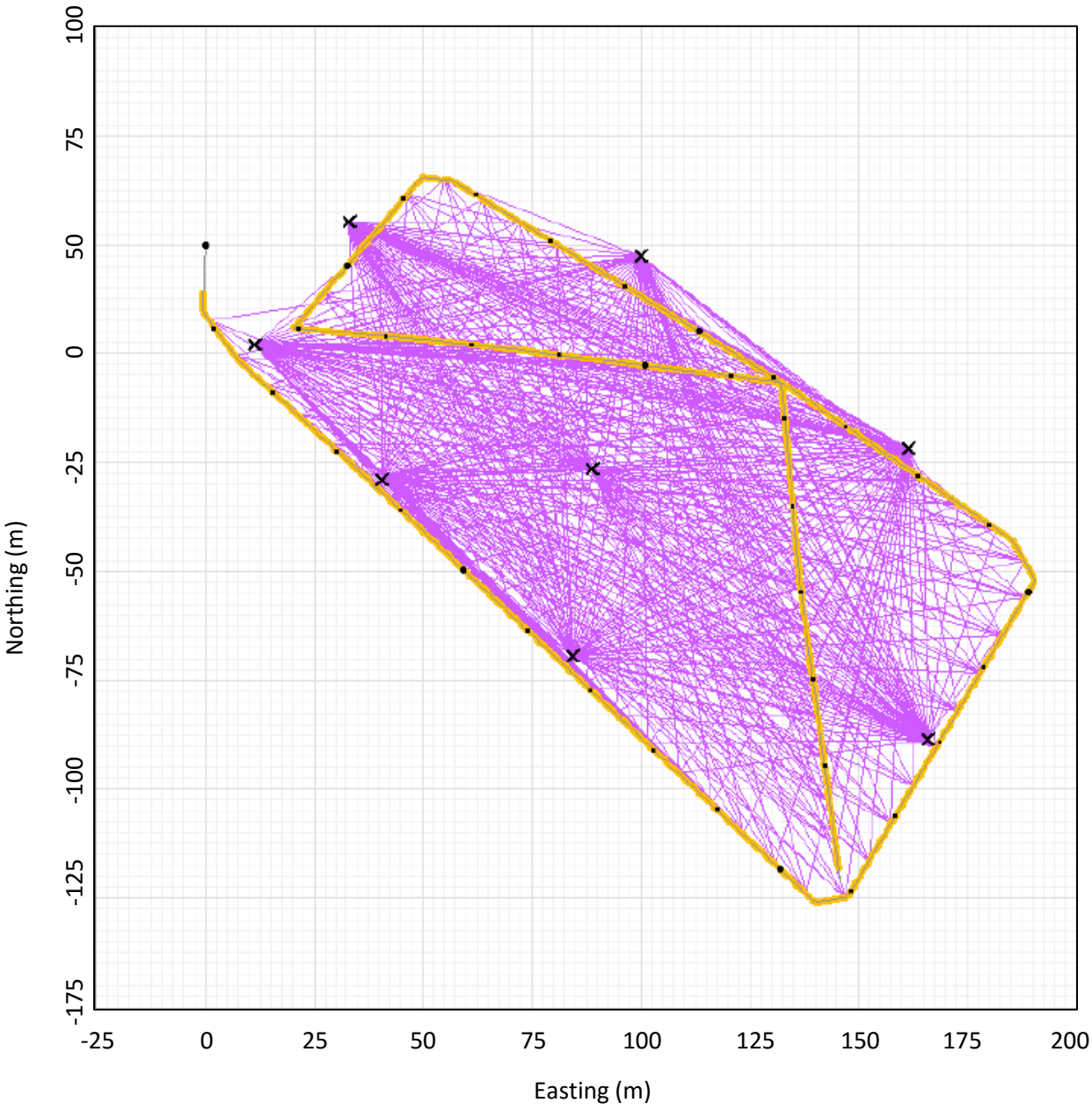

Figure 3.7: Layout of fiber with Vibroseis truck locations marked with x's and ray paths used in the refracted-wave inversion.

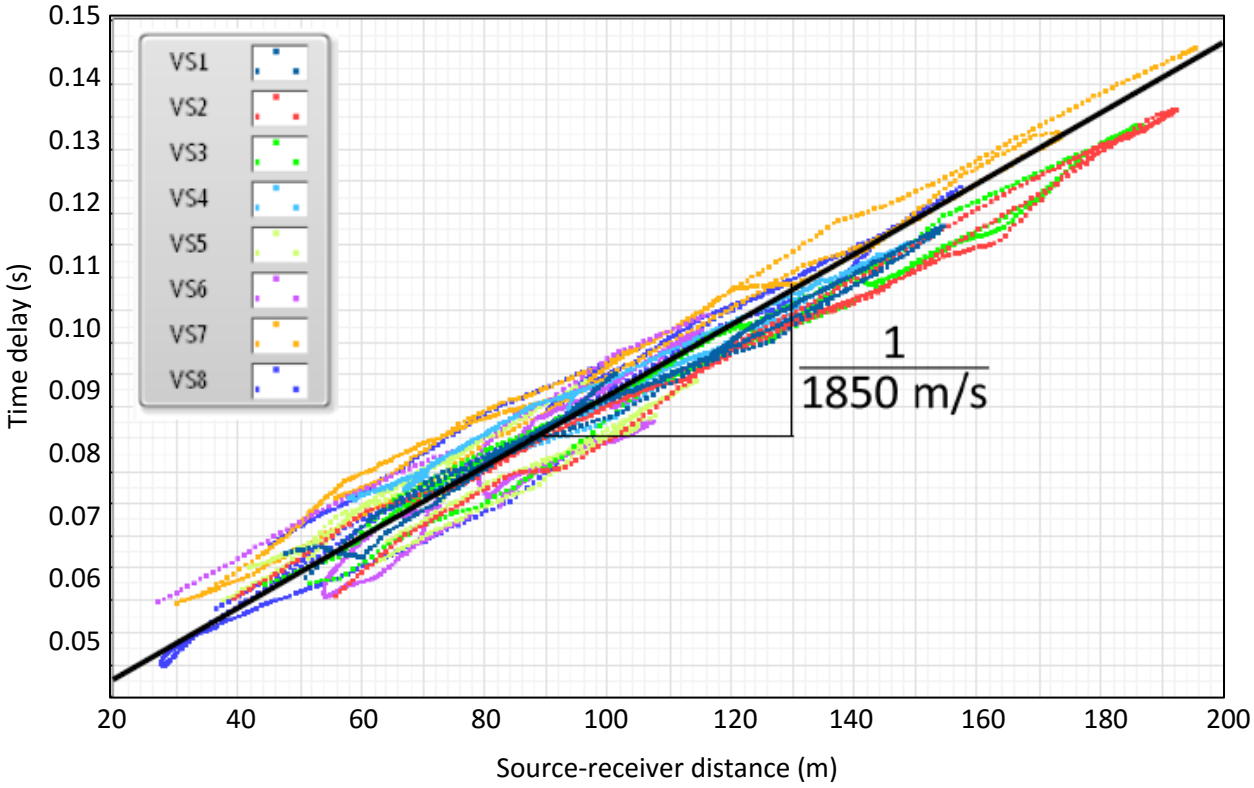

Figure 3.8: Plot of the eight different Vibroseis truck locations and the associated refracted-arrival picks to determine the average velocity and depth of the refracting layer. Each point is one picked arrival time and each color represents a different source (shown in the legend).

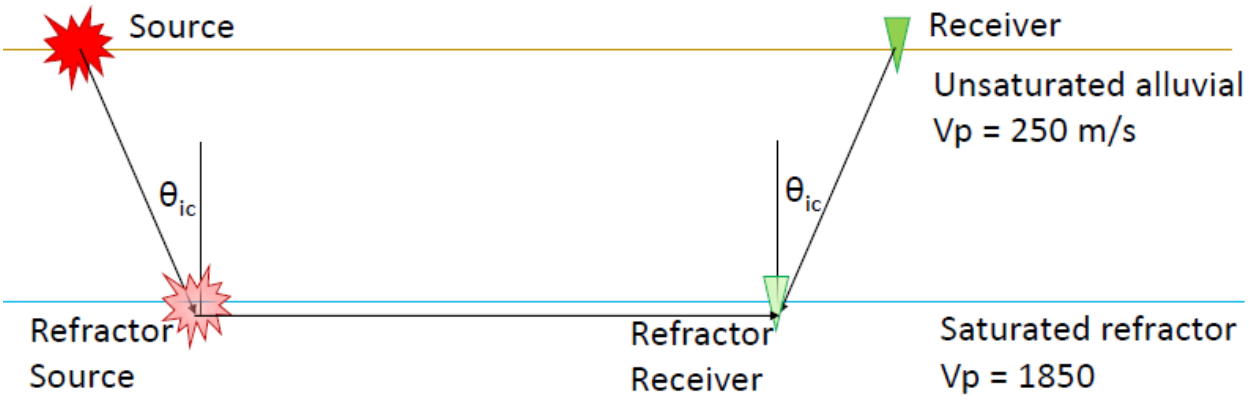

Figure 3.9: Schematic showing calculation of travel times on the refracting layer and relocation of the sources and receivers.

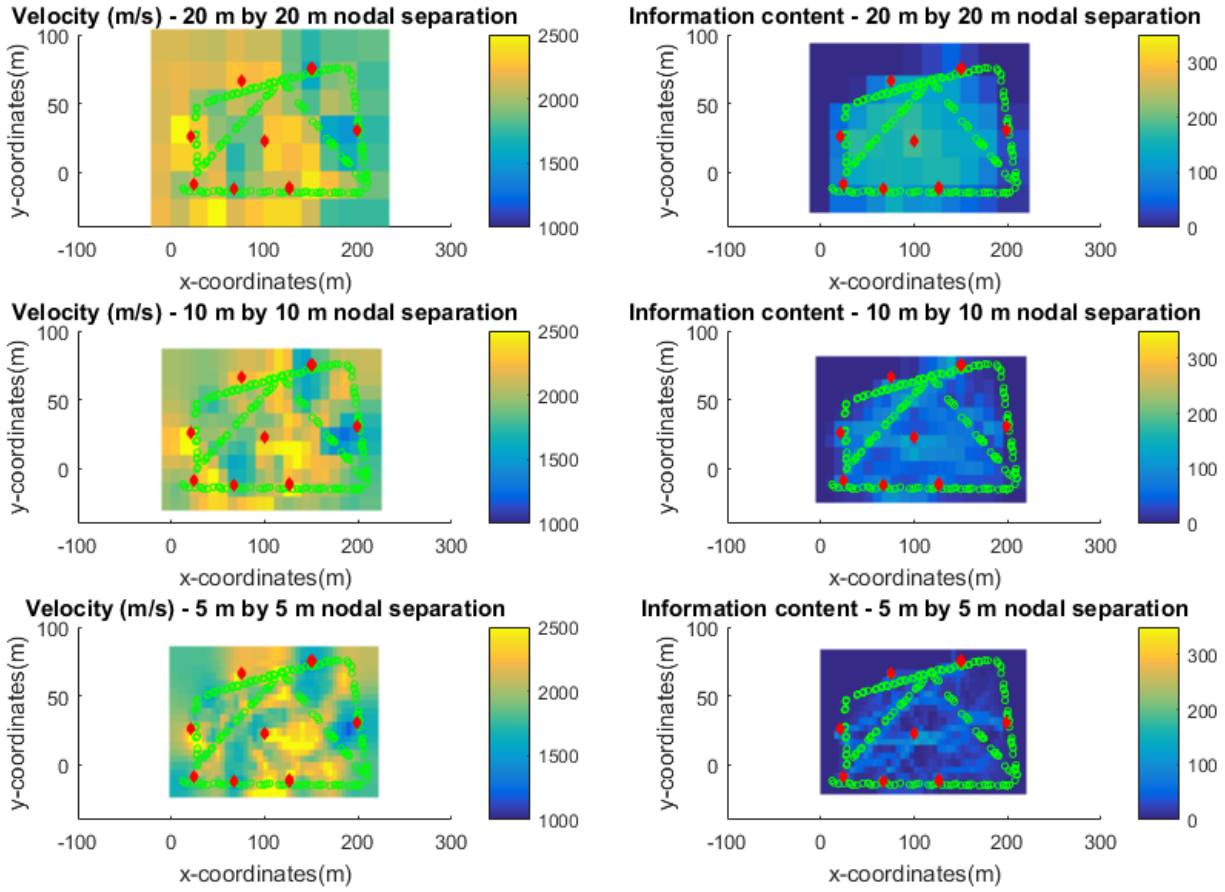

Figure 3.10: Refracted wave inverted velocity fields and the corresponding information content for a 20 m by 20 m (top), 10 m by 10 m (middle), and 5 m by 5 m (bottom) nodal separation.

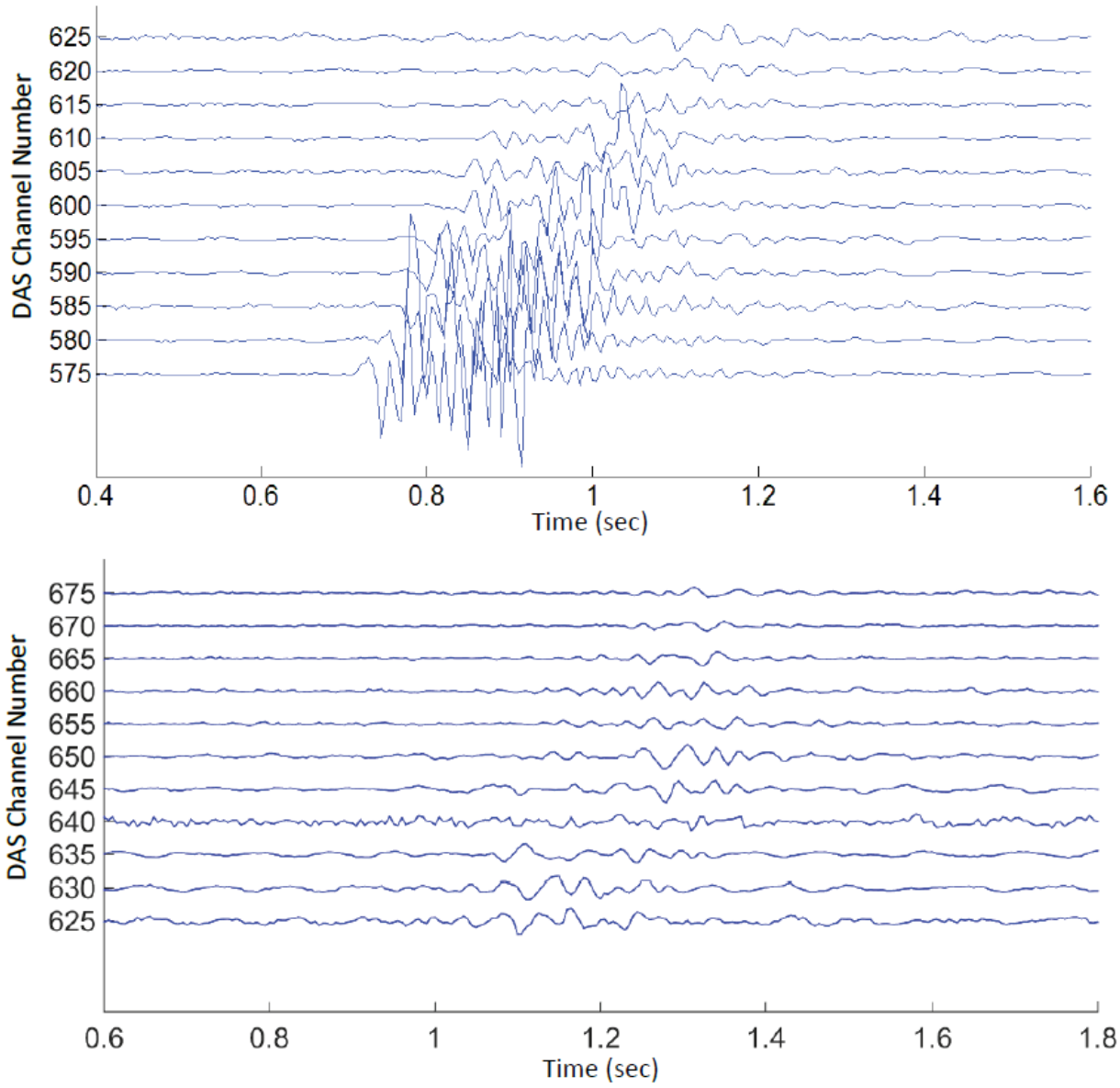

Figure 3.11: Plots of channels in line with (top) and approximately perpendicular to (bottom) particle motion from a hammer blow at location 1. Notice the amplitude of the signal drops off when the particle motion is at a high angle to the cable.

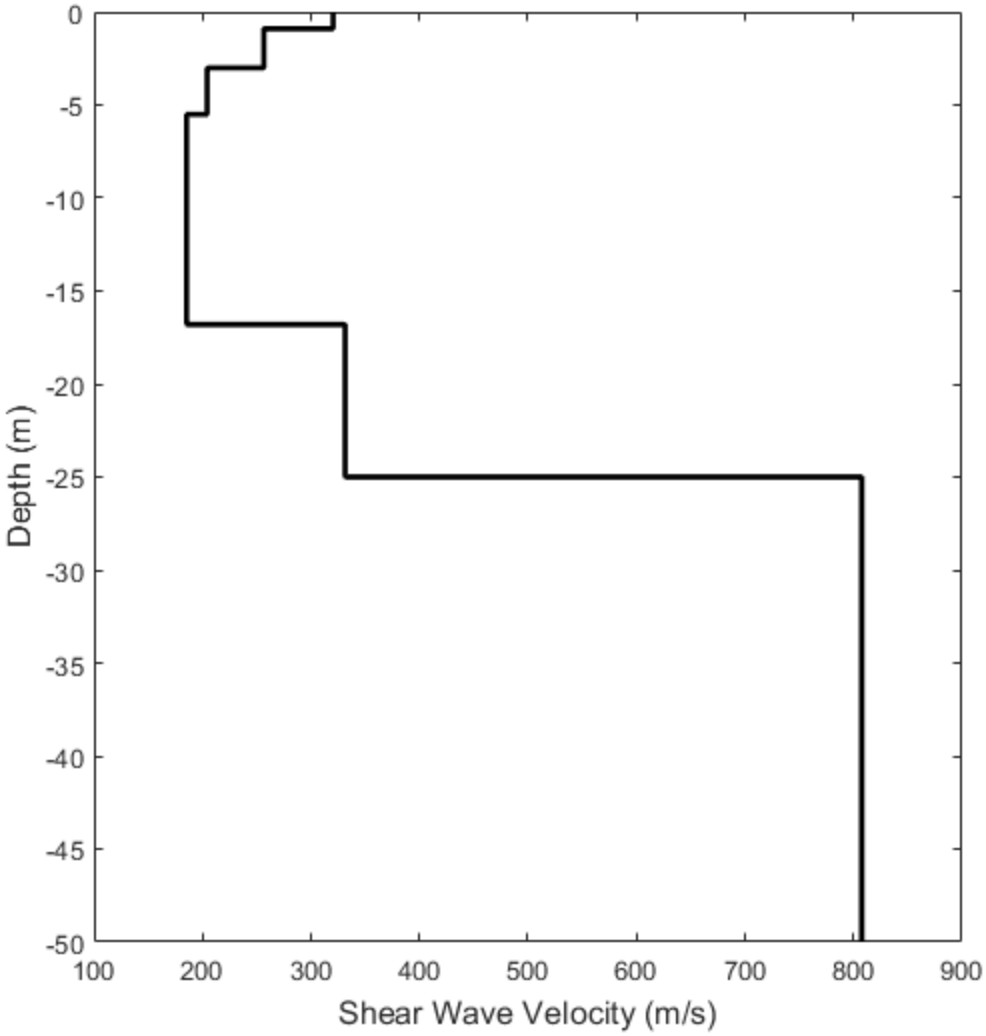

Figure 3.12: MASW results using same DAS array from Lancelle et al. (2016).

Chapter 4

Traffic Monitoring using Distributed Acoustic Sensing (DAS)

Introduction

Monitoring traffic is important for a number of reasons. It allows for better design of future roads and helps in assessing the state of current roads. Understanding the number, size, and weight of vehicles on the roads helps protect the current infrastructure and the environment. Also, real-time information is needed to supply data to intelligent information systems such as electronic road signs and for the real-time assessment of infrastructure health. The earliest traffic monitoring was done in the 1920s using a pneumatic road tube, which is still in use today due to its low cost and simplicity. However, the tube cannot estimate the type or weight of vehicles that pass over it. Since then a number of different traffic monitoring techniques have been used (Gardner 2000).

One reason for traffic monitoring is to get real-time output for alerts or electronic road signs. Video monitoring allows for extraction of traffic loads, lane changes, and average velocities (Semertzidis et al. 2009). Many studies have been done looking at traffic monitoring using video surveillance. There are a few problems with some current intelligent video surveillance techniques. They have issues resolving different types of moving objects or those that are small and poorly textured. Also, video surveillance works poorly in weak or rapidly changing lighting or in shadows (Ji et al. 2006). Most recent studies have focused on improving on the current systems. Ji et al. (2006) developed a background subtraction method, one of a few different ways traffic is detected in videos, to help in poor lighting or shadows. Zhou et al. (2007) developed an algorithm that learns from examples that works well in various conditions,

including shadows and bad illumination. Chen et al. (2011) created a real-time vision system for night-time traffic monitoring that detects vehicle headlights and taillights and groups them into vehicles.

Recently there have been more studies looking at monitoring traffic seismically. Vibrations from traffic are not sensitive to the same issues, such as weather and poor visibility, that hamper video monitoring systems. Riahi and Gerstoft (2015) used an array of 5200 geophones in a 7 km by 10 km area in Long Beach, CA to monitor train, air, and car traffic. They were able to monitor local rail track traffic, aircraft landing at a nearby airport, and nighttime traffic on I-405.

Traffic monitoring can be used to get a better idea of the conditions of the roads. Eriksson et al. (2008) used what they called the "Pothole Patrol" to monitor road conditions and locate potholes in Boston. They used data from accelerometers and GPS sensors attached to taxis to identify areas of concern on the roads. They were able to identify potholes or other areas that caused high vibrations and needed attention at a 90% success rate. Mohan et al. (2008) used smartphones to monitor both traffic conditions and road conditions in cities in developing countries where traffic patterns are not as organized. They developed TrafficSense, which uses a phone's accelerometer, microphone, GSM radio, and/or GPS sensor to monitor for vibrations from potholes, the sounds of honking horns, and braking. TrafficSense was successfully applied in Bangalore, India.

Traffic monitoring is not only important for monitoring roads and traffic, but it is also important in security situations. Border control is one situation where traffic monitoring is important in order to assist law enforcement in monitoring people and vehicles crossing a border region. Coulter et al (2011) utilized light aircraft and unmanned aerial vehicles for repeat

imaging of a border region and were able to identify image changes that occurred when a vehicle or person was present.

Kirkendall et al. (2007) used Distributed Acoustic Sensing (DAS) to monitor borders and pipelines. DAS uses a fiber-optic cable connected to an interrogator box to measure strain rate every meter for distances up to 100 km and at sampling rates as fast as 100 kHz (Johannessen et al. 2012; Miller et al. 2012). The spatial resolution of the DAS system is limited by the gauge length, which is generally on the order of 10 meters. The center of the gauge length is called a channel and the strain rate over the gauge length is attributed to the channel at its center. Kirkendall et al. were able to see footfalls from a person walking perpendicular to the cable as well as a passing convoy of Humvee trucks. Owen et al. (2012) also successfully used DAS for border, pipeline, railway, and high-value facility monitoring and called the DAS system cost effective and efficient in that power and communications are only needed every 80-100 km.

Besides monitoring traffic strictly for traffic information or border control, some studies use traffic as a seismic source. Dikmen et al (2015) used traffic to estimate near-surface attenuation properties. They compared attenuation results from traffic-generated waves to results from earthquake-generated waves and found a similar attenuation using both wave types. Nakata (2016) has used traffic noise to image S-wave velocity distribution in the near surface by capturing and interpreting Rayleigh and Love waves with up 100 geophones.

Zeng et al. (2016) used the same DAS array and data from this study to calculate noise cross-correlation functions (NCFs) for one-minute intervals. The dominant noise in the data was attributed to traffic. The NCFs were used to calculate a dispersion curve using Multichannel Analysis of Surface Waves. The dispersion curve results from the NCFs compared well with those from active sources calculated by Lancelle et al. (2016).

This study evaluates the use of DAS for monitoring traffic. The high spatial sampling and distributed nature of DAS allows for a closer look at the traffic as it passes and how the speed of the vehicle may change over the length of the array. DAS arrays should also be resilient to issues with lighting conditions that video monitoring can have problems with and may be sensitive to the weight of a vehicle, something the pneumatic tube was lacking. This paper will focus on 1) counts of passing vehicles, 2) relative amplitudes between those vehicles, and 3) speeds and directions at one study area in Southern California.

DAS Data Collection

The field site used in this study was the Garner Valley Downhole Array operated by University of California Santa Barbara. It is located in a seismically active zone, 35 km from the San Andreas fault and 7 km from the San Jacinto fault. The geology and geotechnical properties of the site are well known (Youd et al. 2004). It is mostly flat-lying alluvium above weathered and unweathered granitic bedrock. At the site 762 meters of fiber optic cable was trenched approximately 0.3 m deep in a rectangular array with two interior diagonal segments (Figure 4.1). The overall size of the array was approximately 160 m by 80 m. One leg of the array runs approximately parallel to California State Highway 74, the source of traffic in this study. The primary focus of the study was on active tests during the day and passive sources in the evening. The evening data will be used for the traffic analysis in this study.

An example 15-minute data trace from a DAS channel in the NE corner of the array is plotted in Figure 4.2. The raw data are plotted on top and filtered data are plotted on the bottom. A zero-phase, bandpass filter with cutoff frequencies of 0.4 to 15 Hz was used to filter the data in order to remove high-frequency noise not associated with the passing vehicles. The sampling

rate of the DAS data are 1000 samples per second. Figure 4.3 shows the frequency spectrum of the same 15-minute time window. The main frequencies associated with traffic are between 6 and 15 Hz.

Results

Vehicle Counts

Figure 4.2 shows a 15-minute time period recorded by one DAS channel at the NW corner of the array that starts at approximately 6:08 pm local time. Multiple passing vehicles can be seen in the raw data (top), marked by relatively higher amplitude spikes in the data. Filtering the data to remove high frequency noise allows the events, assumed to be caused by passing vehicles, to be seen more clearly (bottom). At this channel, there are 17 relatively high amplitude events over the 15-minute time period.

Looking at a single channel does not allow for separation of two vehicles passing the channel at the same time. In this case, the spatial sampling of DAS allows for multiple points of reference to be evaluated for the number of passing vehicles. Figure 4.4 shows filtered data from every tenth channel along the line running parallel to the road. Using this method allows for individual vehicles to be tracked as they move along the DAS line. In this case there are two vehicles that when looking at just one channel appear to be a single vehicle, but when looking at a number of channels they can be seen as two different vehicles. The first vehicle in the 15-minute window is an example of this (Channel 141.6, Events 1 and 2 in Figure 4.4). At the eastern-most channel, the two vehicles passing in opposite directions are easily identifiable as separate since one vehicle arrives after the other. At the western-most channel, however, the two vehicles are inseparable because their seismic waves arrived at that channel location at the same

time. Looking at the whole DAS line allowed for the determination that there were 18 vehicles that passed this section of the road during the 15-minute time period.

DAS can successfully be used to count passing vehicles when the vehicles are spaced out enough in time to identify them as separate events. However, this study does not give an indication whether DAS could be successfully used to monitor traffic on much busier roads or on highways where multiple lanes of traffic are passing. Future work requiring different sensor arrays and analysis of DAS data where more frequently passing vehicles are prevalent would be required to better assess DAS capabilities.

Relative Amplitudes

As is evident in Figure 4.2, not all passing vehicles have the same amplitude. One possible reason for the difference in amplitudes relates to the direction the vehicle is traveling and thus the distance between the vehicle and the receiver. Figure 4.4 shows multiple channels running from east to west along the road. If one were to follow a vehicle along the DAS line, a positive slope in the plot would indicate the vehicle was traveling from east to west and a negative slope would indicate the vehicle was traveling from west to east. Smaller amplitudes tend to be attributed to vehicles moving east to west and larger amplitudes tend to be attributed to vehicles moving west to east. Vehicles traveling west to east are traveling on the side of the road closer to the DAS line, so it would be logical that their amplitudes would be higher than those of a vehicle traveling on the other side of the road if everything else was held constant.

Another possible reason for the difference in amplitudes between vehicles could be due to vehicle size. A relatively larger vehicle should make a larger amplitude signal. However, this possibility cannot be investigated at Garner Valley because there was not a camera recording traffic.

Vehicle Speeds

DAS data can be used to calculate the speed of the passing vehicles. By analyzing the movement of the vehicles along the DAS line in Figure 4.4, the speed of travel of those vehicles can be calculated. Calculated speeds for all 18 vehicles are shown in Table 4.1. Cars are numbered based on the time of their arrival in the 15-minute window, earlier arrivals first. Directions the vehicles were traveling are also given. Speeds ranged from 19 m/s to 30 m/s.

Figure 4.5 shows a more detailed example of four vehicles, two traveling each direction, and the speed calculation associated with them. Red dashed lines show the average slopes used for the speed calculation. The speed was taken as an average over the 141.57 m distance, although none of the vehicles showed any large increases or decreases in speed over that distance so an average should be a good approximation of the speed. The time difference given in Table 4.1 is based on the two endpoints of the slope line at 0 and 141.57 m. The slope line is fit to all of the channels to make use of the distributed nature of DAS.

Discussion

Vehicle Counts

The DAS results for vehicle counts indicate that DAS can be successful in counting vehicles in some situations. Individual vehicles are identifiable when a line of DAS channels is used, and the same vehicles may have been confused if only point receivers at the beginning and end of the line were used. Even when one channel could not separate two vehicles, the use of consecutive channels allows for separation of two distinct vehicles. However, this study does not test the ability of DAS to identify individual vehicles in high-density traffic areas. The vehicles that crossed over and appeared as one vehicle at one channel were separated by 5 – 10

seconds at another channel before they were considered two separate vehicles. If there were many more vehicles arriving at channels at the same time, separating the vehicles may not be possible and this could be a possible aspect for future study.

Relative Amplitudes

Amplitude differences between vehicles can be attributed to the distance the vehicles are from the cable. In this study area, the cable is running approximately parallel to the road, so a vehicle traveling in one lane will stay approximately the same distance from the cable for the length of the cable. However, it is not perfectly parallel, and this is evident in the change in amplitudes moving from west to east. The cable in the west is slightly closer to the highway than in the east. In the west the cable is about 15 m from the road and in the west the cable is 19 m from the road. In Figure 4.3, the western-most channel has higher overall amplitudes than those from the eastern-most channel because of that slight change in distance from the highway. Surface waves in the frequency range that the vehicles create travel at an average of approximately 200 m/s (Lancelle et al. 2016), meaning it takes about 0.075 seconds for the surface wave arrival to travel the 15 m distance to the western-most channel from the road assuming a homogeneous material. To get to the eastern-most channel from the road it takes about 0.095 seconds.

Most vehicles traveling closer to the cable in the west to east direction have higher amplitudes than those of cars traveling in the east to west direction farther from the cable. Since the DAS results appear sensitive enough to sense amplitude differences due to the distances to each lane, it is possible that DAS could be used to monitor lane changes. However, the cable would need to be perfectly parallel to the road in order do this, and any other sources of increased or decreased amplitude would need to be accounted for. Another possible source of

amplitude differences could be due to the road itself and changing pavement textures, though this is something that was not investigated in this study. Amplitude differences between vehicles could also be attributed to vehicle size or weight, but that possibility cannot be investigated in this study because no record of the size or vehicles, such as a video, was taken.

Vehicle Speeds

Vehicle speeds are calculated using DAS data by following the slope of the traffic signal across multiple channels. In calculating the slope, an assumption was made that the cable was parallel to the road. However, the cable is not parallel. There is a small angle (less than 5 degrees) that is not expected to change the velocities by a significant amount. When calculating the slope, the center of the surface wave arrivals was followed since the signature of the passing vehicle was not the same from channel to channel. The expected difference in arrival times from the closest point on the cable to the road compared to the farthest point on the cable to the road is 0.02 seconds, which is within the 0.05 second picking error.

One benefit of the high spatial sampling of DAS is that there are multiple points of measurement over extended distances. Over the 141.57 m of the length of cable looked at in this study, all vehicles in the 15-minute window traveled at a fairly consistent speed, even when channels two meters apart were plotted. However, tracking vehicles slowing down or speeding up should be possible, since a bend or gradual change in slope would be seen. It should be possible to follow the acceleration and deceleration of a vehicle and the speed at which they accelerate or decelerate. This could give an indication of accidents or traffic jams on a road. While the following of acceleration and deceleration cannot be done in this study because none of the vehicles appeared to accelerate or decelerate, this could be a topic of future study using DAS data.

Another benefit of using DAS for this type of study would be the ease of incorporation into roads. Any time a road was resurfaced or constructed, a fiber-optic cable could be lain out before the pavement. As long as there were access points to attach the interrogator box to the fiber-optic cable, no other set up or coupling would be necessary. In this way no additional cost, besides the cost of the cable and the time it takes to lay it out, would be needed to prepare the DAS array for recording traffic.

Conclusions

The DAS array at Garner Valley successfully recorded vehicles passing on Highway 74. From 15 minutes of data a count of passing vehicles was obtained and the direction and speed of each of the vehicles was calculated. Identification of overlapping vehicles was successfully executed and relative amplitudes give an indication of distance from the cable. Further work could be done to evaluate the ability of DAS to monitor traffic when multiple lanes of traffic are present or in high traffic areas.

References

Chen Y. L., Wu B. F., Huang H. Y., & Fan C. J. 2011. A real-time vision system for nighttime vehicle detection and traffic surveillance. *IEEE Transactions on Industrial Electronics*, *58*(5), 2030-2044.

Coulter L., Lippitt C., Stow D., & McCreight R. 2011. Near real-time change detection for border monitoring. In *Proceedings from the ASPRS annual conference* (pp. 1-5).

Dikmen S. U., Pinar A., & Edincliler A. 2016. Near-surface attenuation using traffic-induced seismic noise at a downhole array. *Journal of Seismology*, *20*(1), 375-384.

Eriksson J., Girod L., Hull B., Newton R., Madden S., & Balakrishnan H. 2008. The pothole patrol: using a mobile sensor network for road surface monitoring. In *Proceedings of the 6th international conference on Mobile systems, applications, and services* (pp. 29-39). ACM.

Gardner M. P. 2000. Highway traffic monitoring. *Transportation Research Board. Transportation in the new millennium*, 5.

Ji X., Wei Z., & Feng Y. 2006. Effective vehicle detection technique for traffic surveillance systems. *Journal of Visual Communication and Image Representation*, *17*(3), 647-658.

Johannessen K., Drakeley B., and Farhadiroushan M. 2012. Distributed Acoustic Sensing - a new way of listening to your well/reservoir, *SPE Intelligent Energy International* held in Utrecht, The Netherlands, 27–29 March 2012, SPE 149602, 9 pp.

Kirkendall C.K., Bartolo R., Salzano J., Daley K. 2007. "Distributed Fiber Optic Sensing for Homeland Security", 2007 NRL Review.

Lancelle C., Baldwin J., Lord N., Fratta D., Chalari A., Wang H. F. 2016. Using Distributed Acoustic Sensing (DAS) for Multichannel Analysis of Surface Waves (MASW) to Evaluate Ground Stiffness, *Near Surface Geophysics* (under review).

Miller D., Parker T., Kashikar S., Todorov M., and Bostick T. 2012. Vertical Seismic Profiling using a fibre-optic cable as a Distributed Acoustic Sensor, 74th EAGE Conference & Exhibition incorporating SPE EUROPEC 2012, Copenhagen, Denmark, 4-7 June 2012, 5 pp.

Mohan P., Padmanabhan V. N., & Ramjee R. 2008. Nericell: rich monitoring of road and traffic conditions using mobile smartphones. In *Proceedings of the 6th ACM conference on Embedded network sensor systems* (pp. 323-336). ACM.

Nakata, N. 2016. Near-surface S-wave velocities estimated from traffic-induced Love waves using seismic interferometry with double beamforming. *Interpretation*. (in press).

Owen A., Duckworth G., and Worsley J. 2012. OptaSense: fibre optic distributed acoustic sensing for border monitoring. In *Intelligence and Security Informatics Conference (EISIC), 2012 European* (pp. 362-364). IEEE.

Riahi N., and Gerstoft P. 2015. The seismic traffic footprint: Tracking trains, aircraft, and cars seismically. *Geophysical Research Letters*, *42*(8), 2674-2681.

Semertzidis T., Dimitropoulos K., Koutsia A., & Grammalidis N. 2010. Video sensor network for real-time traffic monitoring and surveillance. *IET intelligent transport systems*, *4*(2), 103-112.

Youd T. L., Bartholomew H. A. J., and Proctor J. S. 2004. *Geotechnical logs and data from permanently instrumented field sites: Garner Valley Downhole Array (GVDA) and Wildlife Liquefaction Array (WLA)*, Data Report.URL: http://nees.ucsb.edu/sites/eot-dev.nees.ucsb.edu/files/facilities/docs/geotech-data-report.pdf [Accessed on January 9, 2016].

Zeng X., Lancelle C., Thurber C., Fratta D., Wang H. F., Lord N., Chalari A., and Clarke A. 2016. Properties of Noise Cross-correlation Functions Obtained from a Distributed Acoustic Sensing Array at Garner Valley, California, *Bulletin of the Seismological Society of America* (under review).

Zhou J., Gao D., & Zhang D. 2007. Moving vehicle detection for automatic traffic monitoring. *IEEE transactions on vehicular technology*, *56*(1), 51-59.

Tables

Table 4.1: Velocities of Passing Vehicles Averaged over 141.57 m

Event #	Time Difference (s)	Direction Traveling From	Velocity (m/s)	Velocity (mph)
1	5.0	E	28	63
2	5.0	W	28	63
3	6.1	E	23	52
4	5.3	E	27	60
5	5.0	E	28	63
6	6.3	W	22	50
7	5.7	E	25	56
8	5.9	E	24	54
9	7.3	W	19	43
10	6.2	E	23	51
11	6.1	W	23	52
12	6.9	W	21	46
13	5.2	E	27	61
14	4.7	E	30	67
15	7.6	W	19	41
16	6.0	W	24	52
17	6.9	W	21	45
18	7.2	E	20	44

Figures

Figure 4.1: Map of the study area with cable marked with dashed yellow lines. The section of cable parallel to the road is highlighted in blue.

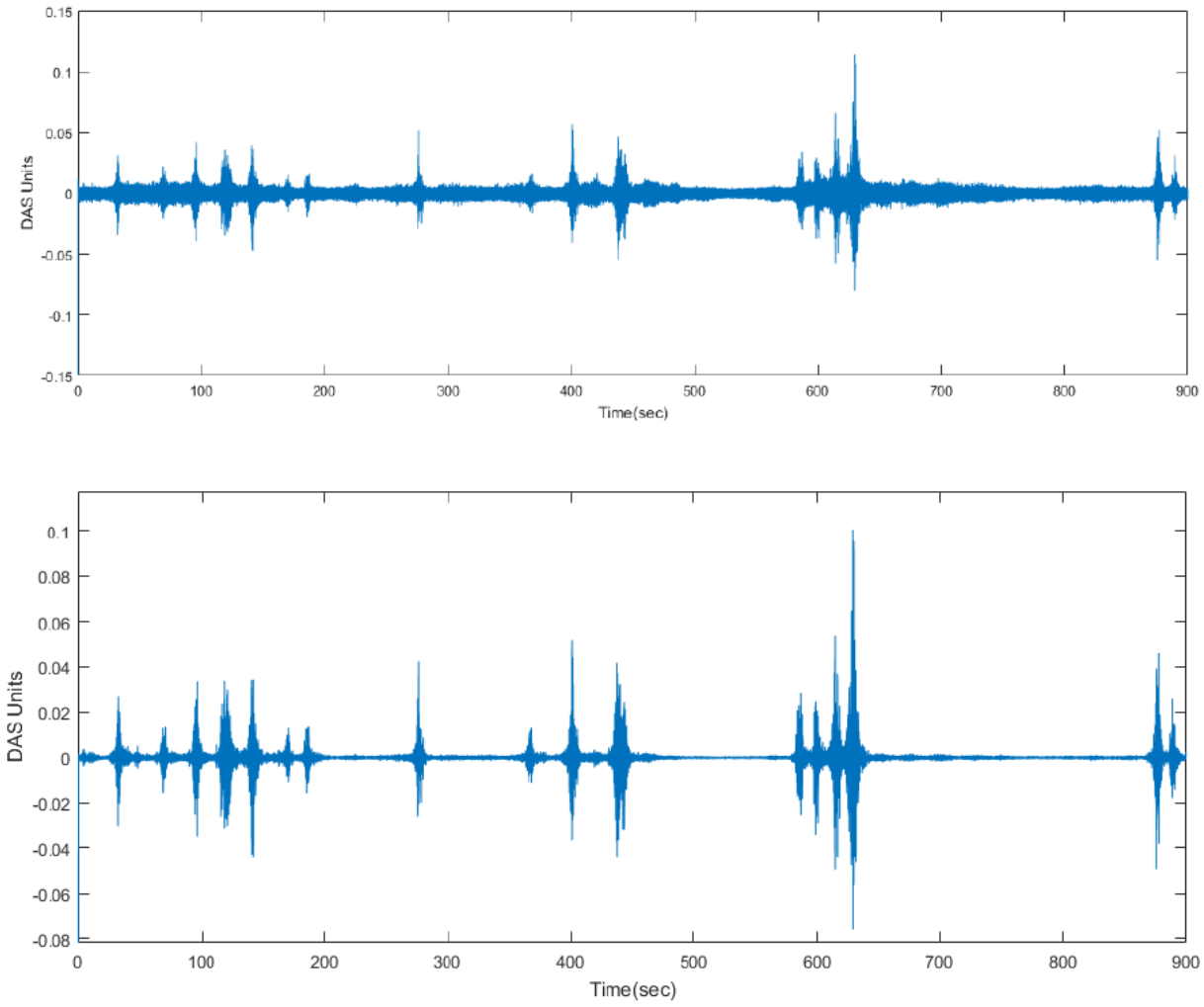

Figure 4.2: Plot of 15 minutes of data from the DAS channel in the NW corner of the array, both raw (top) and zero-phase, bandpass filtered between 0.4 and 15 Hz (bottom).

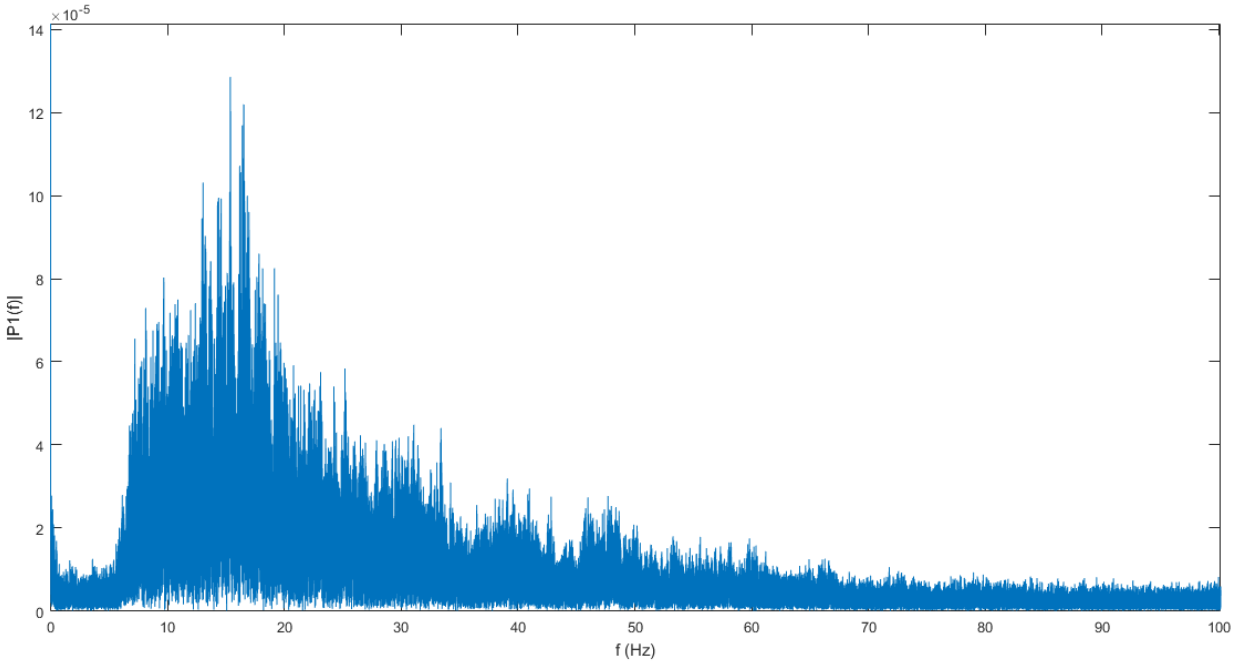

Figure 4.3: Frequency spectrum for the 15-minute time period shown in Figure 4.2.

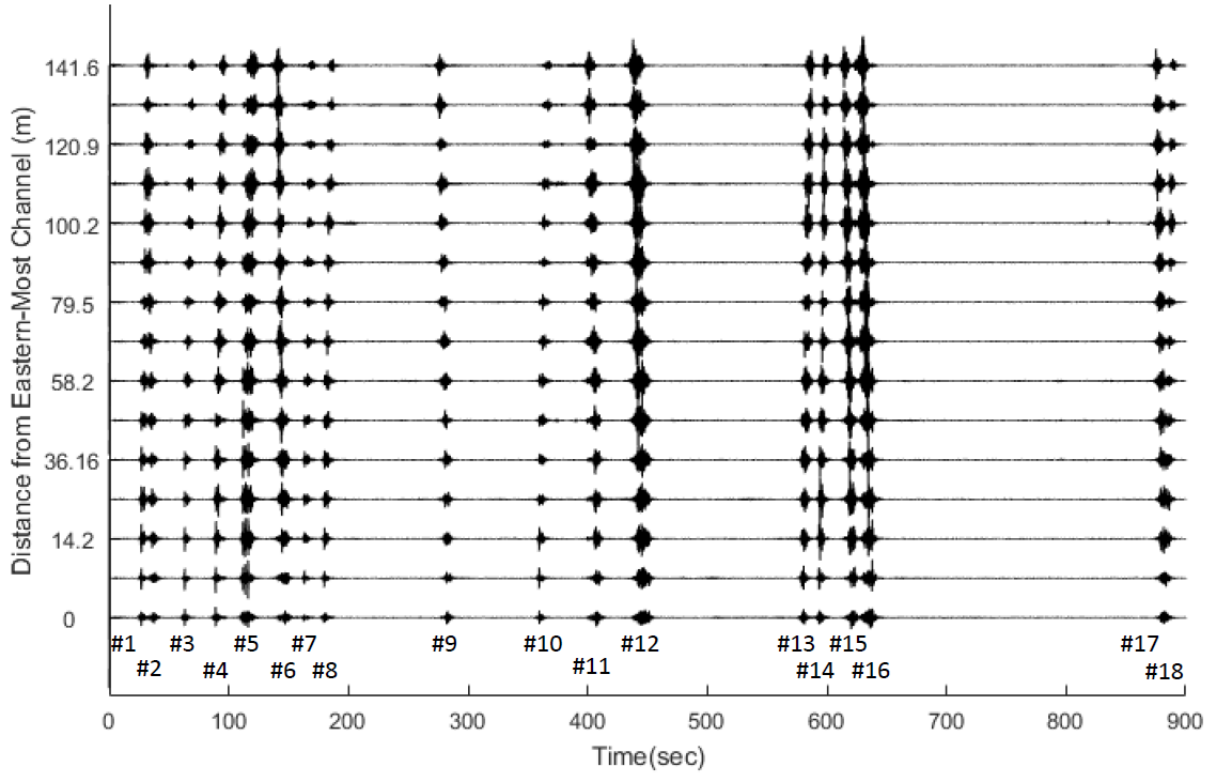

Figure 4.4: Plot of every tenth DAS channel along the line parallel to the road (highlighted in blue in Figure 4.1). Positive slopes indicate an east to west direction, negative slopes indicate a west to east direction. All distances are given from the DAS channel at the NE corner of the array.

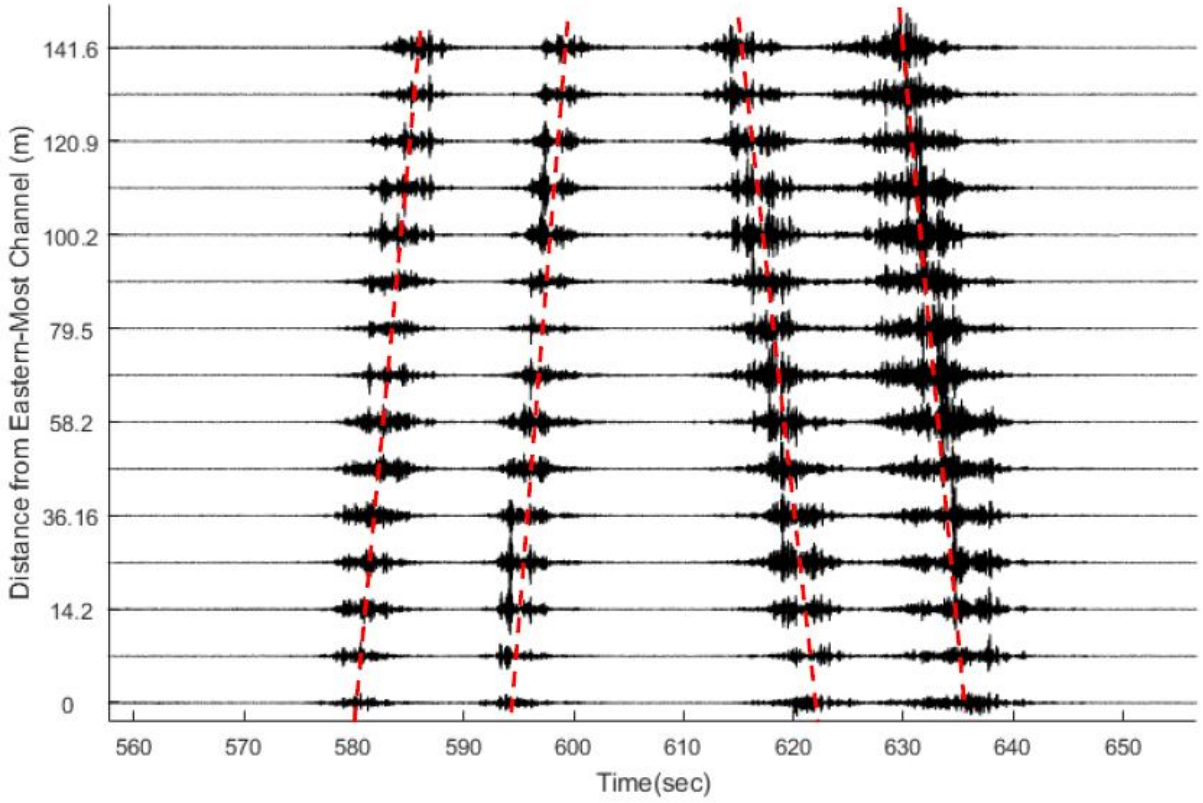

Figure 4.5: Plot of four passing vehicles (#13-16), two in each direction. Slopes following the traffic moveout that were used to calculate the speed of the vehicle are shown with red dashed lines.

Chapter 5

Conclusions

Distributed Acoustic Sensing (DAS) is an exciting new technology that uses a fiber-optic cable attached to an interrogator box as a sensor. While DAS has been used in boreholes for Vertical Seismic Profiling studies, it has less commonly been tested in a horizontal array. This study showed that DAS could be used in a number of different near surface studies that use both surface and body waves.

The DAS array at Garner Valley was successfully used in MASW to create surface wave dispersion curves and ultimately a shear wave velocity profile. The dispersion curves followed the expected trend of decreasing velocity with increasing frequency and matched the dispersion curves from previous studies as well as different analyses from the same array.

Tomographic images were successfully made using the DAS array for three different nodal separation sizes. The resolution of the DAS array out of the three options calculated was 10 m by 10 m since the 5 m by 5 m pixels often had no rays passing through them. Tomographic images were dependent upon the directional sensitivity of the DAS system.

Traffic monitoring using the DAS array was possible. The fiber was able to pick up differences in amplitude between different vehicles and a count of the number of vehicles passing in a specific period of time could be established. Also, the speed of the vehicles could be determined.

In all of these studies an understanding of the directional sensitivity of DAS is very important. Since the cable is only sensitive to strain along its length, care needs to be taken

when designing future studies. Aligning the cable with the direction of particle motion will give the best results, though as shown in this study, even at a relatively high angle to the fiber a signal can still be seen.

Future studies of DAS could further investigate the directional sensitivity of the DAS system. The interaction between the cable and particle motion incoming at high angles to the cable could be better investigated to see if there is a "cutoff" angle above which DAS data should not be used. The effects of the gauge length on results is also a topic that could warrant further research. Since gauge length is essentially a moving-average filter over, in this case, 10 m, there may be some smoothing that happens because of the gauge length.

One future study that could investigate these topics is the PoroTomo project at Bradys Hot Springs in Nevada. The size of this DAS array was an order of magnitude smaller than the Bradys study. There, rather than using 762 meters of cable, the DAS array used 9 kilometers of cable in combination with nodal seismic instruments. Also, rather than a fully horizontal array, a segment of cable was in a borehole. All of the analyses from this study could, and plan to be, carried out as part of that study.

This Garner Valley study was used as a launching pad for the PoroTomo study. The planning of the horizontal array and the locations of sources with respect to the fiber were based on lessons learned at the Garner Valley site. The field work for the PoroTomo project was completed in March 2016 and analysis of that data is underway.

Appendix

Matlab Scripts used for MASW Analysis

MASW_SSF.m

```
%% Source Synchronous Filtering Script

% sampling rate
fs=1000;

%indexes into gv dataset
trigin=5;
trigout=13;
foot=9;
timeindex=1;

% load the data files
% source
granitefile='20130910231307.UCLAGR2.txt';
granitepath='.';
load('GR2_130910231307')
% receivers
load('LS_DAS_130910161319')

granitedata=importdata(fullfile(granitepath,granitefile));
timedata=granitedata(:,timeindex);
timedata=timedata/86400 + 719529; %convert to matlab time

% source data ******************************************
granitewf=waveform(granitedata(:,foot),timedata); % make a waveform
object from the data
triggerwf=waveform(granitedata(:,trigin),timedata); % make a waveform
from the trigger data
triggertime=gettrig(triggerwf); % get the trigger time

% sourcewf=makesourcesweep(timepts,freqpts,fs,delay,triggertime)
sourcewf=makesourcesweep([0 30 60],[0 10 0],fs,0,triggertime);% make
synthetic source phase angle data

% get acceleration data
accel = GR2(:,3);
% calculate cumulative velocity
vel_1 = cumtrapz(accel);
%calculate velocity at each individual time point
for i = 2:length(accel)
    vel(i) = (vel_1(i)-vel_1(i-1))*0.001;
end
% calculate cumulative displacement
```

```
disp_1= cumtrapz(vel);
% calculate displacement at each individual time point
for i = 2:length(vel)
    disp(i) = (disp_1(i)-disp_1(i-1))*0.001;
end

% define filters for SSF
narrowfilter=zerophasebutter(350,2,8);
initfilter=zerophasebutter((30+.4)/2,(30-.4),8);

% apply ssf
%
res=ssf(wavesin,fs,initialfilterparams,narrowfilterparams,sourcewavefo
rm);
% wavesin:    Waves in can be one of 3 possibilities:
%             1) an array of waveforms arrainged as columns, all with
the same
%             time base - timebase must be the same as the source
waveform
%             2) a single object of the 'waveform' class
%             3) a cell array of multiple 'waveform' class objects -
each
%             can have a unique timebase.
%
%  Filter definitions may be either an object of the 'zerophasebutter'
class OR a 3
%  element vector defining the centerfrequency, width and order to be
used
%    i.e.:  narrowfilter=zerophasebutter(350,80,8); % define
zerophasebutter object
%
%    or
%           narrowfilter=[350,80,8]
% exampe if wf1, wf2, wf3 are waveform sources
% res=ssf({wf1,wf2,wf3},fs,initfilter,narrowfilter,sourcewf);

% filter iDAS data
filtiDAS = zeros(60000,35);
% DAS file 130910161319
iDAStimedata = timedata(60753:123752);

% plot 30 m of long line starting at channel 230
start_chan = 230;
for j = 1:31
    sampdowniDAS = resample(LS_DAS(:,start_chan+j-1),5,1);
    DC = mean(sampdowniDAS);
    DCrem = sampdowniDAS-DC;
    % receiver data
    iDASwf = waveform(DCrem,iDAStimedata);
    %    iDASwf = waveform(sampdowniDAS,iDAStimedata);
    res=ssf(iDASwf,fs,initfilter,narrowfilter,sourcewf);
    % filtered receiver
```

```
    filtiDAS_no_AGC(:,j) = res.y;
    [filtiDAS(:,j),env_DAS,gn_DAS] =
Moving_AGC(filtiDAS_no_AGC(:,j),1000);
    tiDAS(:,j) = res.timevec;
end

% filter source data
dispwf = waveform(disp(60753:123752)',iDAStimedata);
res = ssf(dispwf, fs, initfilter, narrowfilter, sourcewf);
% filtered source
filtdisp = res.y;

%% Take small "chunk" of source to cross-correlate for MWCC
% chunk of source to cross correlate
start_time = 5000;
filtchunk = filtdisp(start_time:start_time+2000);

% taper the chunk using tukey window
hwin = tukeywin(length(filtchunk),0.2);

for j = 1:length(filtchunk)
        tapchunk_no_AGC(j) = filtchunk(j)*hwin(j);
end

[tapchunk,env,gn] = Moving_AGC(tapchunk_no_AGC',200);

%% Cross-Correlate

for i = 1:31
   corrsig(:,i) = xcorr(filtiDAS(:,i)-mean(filtiDAS(:,i)),tapchunk-
mean(tapchunk));
end

%% Plotting filtered traces
offset = 1;
tiDAS = 0:0.001:120-0.002;
figure
realoffset = 10;

% loop through the channels
[m,maxindex] = max(corrsig(:,10));
start_index = maxindex - 2000;
stop_index = maxindex + 2000;
for k = 1:5:31
    if k > 1
        offset = offset + 2000;
    end
    hold on

shade_anomaly(tiDAS(start_index:stop_index)',(corrsig(start_index:stop
_index,k))+offset,'b',offset);
    ylim([-2000 14000])
```

```
    xlim([start_index/1000+1 stop_index/1000-1])
    xlabel('Time from Start of Sweep (sec)')
    ylabel('Distance from Source (m)')
end
k
hold off
xlim([64.4 66.4])
set(gca,'YTick',[0 2000 4000 6000 8000 10000 12000] );
set(gca,'YTickLabel',[61.1 65.6 70.1 74.6 79.1 83.6 88.1] );
set(gca,'XTick',[64.4 64.6 64.8 65 65.2 65.4 65.6 65.8 66 66.2 66.4]);
set(gca,'XTickLabel',[5 5.2 5.4 5.6 5.8 6 6.2 6.4 6.6 6.8 7]);
```

All following codes are written by Peter Sobol at University of Wisconsin Madison based on a filtering technique created by Neal Lord, also at University of Wisconsin Madison:

Lord N., Wang H. F., and Fratta D. 2016. A Source-Synchronous Filter for Uncorrelated Receiver Traces from a Swept-Frequency Seismic Source, *Geophysics* (in press).

ssf.m

```
function
resultwf=ssf(wavesin,fs,initialfilter,narrowfilter,sourcerevs)
%function
resultwf=ssf(wavesin,fs,initialfilter,narrowfilter,sourcerevs,encoderp
osition)
% Wrapper for source synchronous filter function.  This function
% pre-processes the data and forms a time union of the data and
sourcerev
% data.
%
% inputs:
% wavesin:    Waves in can be one of 3 possibilities:

%             1) a single object of the 'waveform' class
%             2) a cell array of multiple 'waveform' class objects -
each
%             can have a unique timebase.
%             3) an array of waveforms arrainged as columns, all with
the same
%             time base (in this case no time union will be performed
-
%             sourcerevs must have the same timebase!)
%
% fs:          sampling frequency
%
% initfilter:  filter definition for initial prefiltering of the data
%
```

```
% narrowfilter: filter definition for the narrow band filter used on
the
%               modulated data
%
%  Filter definitions may be either an object of the 'zerophasebutter'
class OR a 3
%  element vector defining the centerfrequency, width and order to be
used
%    i.e.:  narrowfilter=zerophasebutter(350,80,8); % define
zerophasebutter object
%    or
%           narrowfilter=[350,80,8]
%
% sourcerevs: an object of the waveform class containing a vector of
source
%             positions.
% triggertime:

%% input checks
 % check& create filters
if ~isa(initialfilter,'zerophasebutter')% filter is not predefined as
a class
    if isa(initialfilter,'double') && length(initialfilter)==3; % if
its a 3 element vector then define filter

initialfilter=zerophasebutter(initialfilter(1),initialfilter(2),initia
lfilter(3));
    else
       error('Initialfilter must be an object of class
''zerophasebutter'' or a 3 element vector [centerfrequency, width,
order]');
    end
end

if ~isa(narrowfilter,'zerophasebutter')% filter is not predefined as a
class
    if isa(narrowfilter,'double') && length(narrowfilter)==3; % if its
a 3 element vector then define filter

narrowfilter=zerophasebutter(narrowfilter(1),narrowfilter(2),narrowfil
ter(3));
    else
       error('Narrowfilterfilter must be an object of class
''zerophasebutter'' or a 3 element vector [centerfrequency, width,
order]');
    end
end

%%
 mintime=min(sourcerevs.timevec);maxtime=max(sourcerevs.timevec);

 %% check and parse waveform data
```

```
 if isnumeric(wavesin); % data passed is a set of waveforms all with
the same time base as columns in a single array.
            data=wavesin;
 else
     if isa(wavesin,'waveform'); % single set of data passed as a
waveform object
          wavesin={wavesin};
     end
        % fs=1/wavesin.dt;

     if isa(wavesin,'cell'); % multiple waveforms with different time
bases
         % multiple data sets need to unioned along the same time base

         for i=1:length(wavesin);
            if ~isa(wavesin{i},'waveform');
                error('For multiple waveforms, all cells must contain
''waveform'' objects')
            end
            if wavesin{i}.dt ~=1/fs; % need to resample (maybe)
                fsi=1/wavesin{i}.dt;
                    fsi=fsi*1e4;
                    fsi=[floor(fsi) ceil(fsi)]/1e4;
                    if floor(fsi)<=fs & fs<=ceil(fsi);% if its in
rounded range then all good

                    else % need to resample
                        error('All waveforms need the same sampling
frequency');
                        %XXX add resampling code here.
                        %
                       %  wavesin{i}.resample(1/fs);% resample to the
new sample interval
                    end
            end

             mintime=[mintime wavesin{i}.timevec(1)];
             maxtime=[maxtime wavesin{i}.timevec(end)];
         end

          if any(mintime ~= max(mintime)) || any(maxtime ~=
min(maxtime)) % need to unionize the data
             mintime=max(mintime);maxtime=min(maxtime);
             if ~maxtime>mintime;
                 error('Datasets do not have overlapping time bases');
             end

             for i=1:length(wavesin);
                 wavesin{i}=wavesin{i}.trim([mintime maxtime]); % trim
each waveform

             end
```

```
          end
          data=[];timevec=[];
           for i=1:length(wavesin);
               try
                timevec=[timevec wavesin{i}.timevec];
                data=[data wavesin{i}.y];
               catch
                   error(['Error unionizing waveforms, dataset '
num2str(i) ]);
               end
           end

         sourcerevs=trim(sourcerevs,[mintime maxtime]);
         sourcedata=sourcerevs.y;
     end
 end

%%
% end input checks

%% generate source phaseangle vector if necessary
%figure(3)
%subplot(2,1,1);plot(data);
% original
result=ssf1(data,fs,initialfilter,narrowfilter,sourcedata);
%modified
%result =
ssf1(data,fs,initialfilter,narrowfilter,sourcedata,encoderposition);
resultwf=waveform(result,sourcerevs.timevec);
%subplot(2,1,2);plot(result);
%linkaxes
```

ssf1.m

```
function
result=ssf1(waveformin,fs,initialfilter,narrowfilter,sourceposition)

% Source Synchrounous Filter function
%
%inputs:
% wavesin:     set of input waveforms in an array arrainged as columns
% fs:          sampling frequency
% initfilter:  filter definition for initial prefiltering of the data
% narrowfilter: filter definition for the narrow band filter used on
the
%               modulated data
% sourceposition:   Vector of source positions correlated with the
input waveforms
```

```
% Filter definitions:  each of these is structure used to define the
%                   properties of the filters applied to the
waveforms.
%                   Each filter structure should have 3 fields:
%                     .centerfreq  - center frequency in hz
%                     .width       - width in hz
%                     .order       - filter order.
%          example:  Define a filter with a center @350hz, width of
80hz and order 8;
%                      narrowfilter.centerfreq=350;
%                      narrowfilter.width=80;
%                      narrowfilter.order=8;

%% generate the phase data from the sourceposition
% original
    [re im]= rev2phase(sourceposition,fs,narrowfilter.centerfreq);

  % apply the initial filter
    wave=initialfilter.filter(waveformin,fs);

    %xlswrite('Matlab_Labview_Comparison',wave,'After Initial
BPF','T3');

% look at power spectrum from the initial filtered result
    %    figure(10)
%delta_f=fs/length(wave);
%f=-fs/2:delta_f:fs/2-delta_f;
%tilt_w=fft(wave);
%set(gca,'fontsize',14)
%plot(f,fftshift(abs(tilt_w)),'Linewidth',2)
%xlabel('Frequency (Hz)')
%ylabel('Amplitude')

  % calculate the hilber transform
     hwave=hilbert(wave);

   % filter the modulated data
     cwave=narrowfilter.filter(bsxfun(@times,real(hwave),re)-
bsxfun(@times,imag(hwave),im),fs);
   % calculate the hilbert transform
     hwave=hilbert(cwave);
%
%    % demodulate the waveforms
     result=
bsxfun(@times,real(hwave),re)+bsxfun(@times,imag(hwave),im);

function [re im]=rev2phase(rev,fs,centerfreq)
% calculate local oscillator phase angle
% inputs: rev- revolutions
% fs: time interval of points in rev
% CenterFreq:
% outputs: [re im] - real and imaginary parts of the phase angle
```

```
rev=rev(:)';
accum=[0:length(rev)-1]*centerfreq/fs;

wave=(accum-rev)*2*pi();

[re im]=pol2cart(wave,1);
re=re';im=im';
```

filtzerophaseband.m

```
function out=filtzerophaseband(in,fs,filterspec);

% filterspec is a 3-element struction with fields UpperCut, LowerCut
and
% dt is sampleing freq. of wave

%build the filter design

lowercut=filterspec.centerfreq-filterspec.width/2;
uppercut=filterspec.centerfreq+filterspec.width/2;

[b a]=butter(filterspec.order/2,[lowercut uppercut].*2/fs,'bandpass');
%normalized frequency

out=filtfilt(b,a,in);
```

makesourcesweep.m

```
function sourcerevs=makesourcesweep(time,freq,fs,delay,triggertime);

% inputs:
% time:         vector of times at which frequencies are specified
% freq:         vector of frequencies at each time
%
%     time and freq MUST be the same length.
%
% fs:           sampling frequency
% delay:        initial delay time for source
% triggertime:  time of trigger in matlab datenum format

% outputs:
%     sourcerevs: waveform object

time=time(:);freq=freq(:);
if length(time)~=length(freq);
    error('Time and frequency vectors must be the same length!');
```

```
end

if ~exist('delay') || isempty(delay);
    delay =0;
end

sweepvec=[];timevec=[];
for i=1:length(time)-1;

    temptime=time(i):1/fs:time(i+1);
    tempsweep=linspace(freq(i),freq(i+1),length(temptime));

    timevec=[timevec temptime(1:end-1)];
    sweepvec=[sweepvec tempsweep(1:end-1)];

end

sweepvec=cumsum(sweepvec)/fs;
sourcerevs=waveform(sweepvec',+triggertime+(timevec+delay)'/86400);
```

rev2phase.m

```
function [re im]=rev2phase(rev,fs,centerfreq)
% calculate local oscillator phase angle
% inputs: rev- revolutions
% dt: time interval of points in rev
% CenterFreq:

accum=[0:length(rev)-1]*centerfreq/fs;

wave=(accum-rev)*2*pi();

[re im]=pol2cart(wave,1);
```

waveform.m

```
classdef waveform
%    Waveform class is designed to hold timeseries data
    properties
        t0      % time of first datapoint as matlab datenum
        dt      % interval between datapoints in seconds
        y       % waveforms arrainged as an array with each waveform a
seperate column
        timevec % vector of time points expressed as matlab datenums
    end
    methods
```

```
        function obj=waveform(y,varargin) % class constructor
            if nargin==2; % timevector passed
                tv=varargin{1};
                tv=tv(:);
                if size(tv,1)==size(y,1);% good time vector
                    obj.y=y;
                    obj.t0=tv(1);
                    obj.timevec=tv;
                    obj.dt=(tv(end)-tv(1))./(size(tv,1)-1)*86400;

                else
                    error('Time vector must be the same length as
waveform data')
                end
            elseif nargin==3; % to and dt passed
                obj.y=y;
                obj.t0=varargin{1};
                obj.dt=varargin{2};
                obj.timevec=[0:size(y,1)-1]'*obj.dt/86400+obj.t0;
            else
                error('Incorrect # of arguments, supply a time vector
or t0 and dt');
            end
        end
        function obj=maket0(obj); % recalculate t0

            obj.t0=obj.timevec(1);

        end
        function obj=resample(obj,newdt)

newtimevec=[min(obj.timevec):newdt/86400:max(obj.timevec)];

        end
        function obj=trim(obj,minmax)
            newtimeindex=(obj.timevec>=min(minmax) & obj.timevec <=
max(minmax));
            if ~sum(newtimeindex) % no values match
            error('No values in time range')
            end
                obj.timevec=obj.timevec(newtimeindex);
            obj.y=obj.y(newtimeindex,:);
            obj=obj.maket0;

        end
        function obj=normalize(obj);
            obj=meancenter(obj);
            obj.y=obj.y/(max(obj.y)-min(obj.y));
        end
        function obj=meancenter(obj);
              obj.y=obj.y-mean(obj.y);
        end
```

```
        function trigtime=gettrig(obj);
            % extract "trigger time" from the data.  This is the first
            % point at which the amplitude of the waveform exceeds 50%
of
            % its maximum amplitude.
            trigdata=normalize(obj);

            trigindex=find(trigdata.y>=0,1);
            trigtime=obj.timevec(trigindex);

        end
        function out=mintime(obj);
            out=min(obj.timevec);
        end
        function out=maxtime(obj);
            out=max(obj.timevec);
        end
        function plot(obj)
            plot(obj.timevec,obj.y);
            datetick('x');
        end
    end
end
```

zerophasebutter.m

```
classdef zerophasebutter
    % zerophasebutter:  classdef for implementing zerophase
butterworth
    % filter.
    % use obj=zerophasebutter(centerfreq,width,order) to define a
filter
    % out= obj.filter(waveforms) to apply a zerophasefilter to the
input
    % waveforms

    properties
        centerfreq
        width
        order
        uppercut
        lowercut
        fs % sampling frequency
        b % filter parameters
        a % filter parameters
    end
```

```
    methods
        function obj=zerophasebutter(centerfreq,width,order);

            if nargin<3;
                obj.centerfreq=[];
                obj.width=[];
                obj.order=[];
                 error('Three parameters needed (centerfreq, width,
order) to define filter!');
            else
                obj.b=[];
                obj.a=[];
                obj.centerfreq=centerfreq;
                obj.width=width;
                obj.order=order;
                obj.uppercut=centerfreq+width/2;
                obj.lowercut=centerfreq-width/2;
                if obj.lowercut<=0;
                    error('Center frequency must be greater than
width/2');
                end
            end
        end
        function obj=calcloweruppper(obj);
                obj.uppercut=obj.centerfreq+obj.width/2;
                obj.lowercut=obj.centerfreq-obj.width/2;
        end
            function obj=makebutter(obj,fs)
                if obj.uppercut>fs/2;
                    error('Centerfreq + width/2 must be less than
fs/2');
                else
                obj=obj.calcloweruppper;
                [obj.b,obj.a]=butter(obj.order/2,[obj.lowercut
obj.uppercut].*2/fs,'bandpass');
                end
            end

        function results=filter(obj,waveforms,fs);
            obj=obj.makebutter(fs);
            %Using filtfilt - original
            results=filtfilt(obj.b,obj.a,waveforms);

            %Manually recreating filtfilt
            %y = filter(obj.b,obj.a,waveforms);
            %yf = flipud(y);
            %zf = filter(obj.b,obj.a,yf);
            %results = flipud(zf)
        end
    end
end
```